Floating Tangents for Approximating Spatial Curves with G^1 Piecewise Helices

Alexandre Derouet-Jourdan, Florence Bertails-Descoubes, Joëlle Thollot

INRIA and Laboratoire Jean Kuntzmann, (Grenoble University, CNRS), France

Abstract

Curves are widely used in computer science to describe real-life objects such as slender deformable structures. Using only 3 parameters per element, piecewise helices offer an interesting and compact way of representing digital curves. In this paper, we present a robust and fast algorithm to approximate Bézier curves with G^1 piecewise helices. Our approximation algorithm takes a Bézier spline as input along with an integer N and returns a piecewise helix with N elements that closely approximates the input curve. The key idea of our method is to take $N + 1$ evenly distributed points along the curve, together with their tangents, and interpolate these tangents with helices by slightly relaxing the points. Building on previous work, we generalize Ghosh's proof for the co-helicity condition, which serves us to guarantee the correctness of our algorithm in the general case. Finally, we demonstrate both the efficiency and robustness of our method by successfully applying it to various datasets of increasing complexity, ranging from synthetic curves created by an artist to automatic image-based reconstructions of real data such as hair, heart muscular fibers or magnetic field lines of a star.

Keywords: Curve approximation, piecewise helix, G^1 continuity, tangents interpolation

Email addresses: `alexandre.derouet-jourdan@inria.fr` (Alexandre Derouet-Jourdan), `florence.descoubes@inria.fr` (Florence Bertails-Descoubes), `joelle.thollot@inria.fr` (Joëlle Thollot)

Figure 1: Helical shapes in nature emerging from the structure of vine tendrils (left, credits: Jon Sullivan, pdphoto.org), hair ringlets (middle, credits: F. Bertails-Descoubes), and DNA (right, credits: Wikipedia).

1. Introduction

Many real-world objects such as hair, wires, roads, biological filaments or plant stems can be viewed as *1d slender structures*, for which the thickness is negligible compared to the length. Most of those structures exhibit a smooth, bendy shape that often takes the form of *helices* (see Figure 1), which, from a physical viewpoint, can be understood as spontaneous equilibrium configurations in the presence of bending and twisting energies [7]. In this paper we are interested in the digital representation of smooth curves with a compact yet accurate geometric primitive. Motivated by the profusion of helix-like shapes in nature, we made our choice on G^1 *piecewise circular helices* (simply referred to as *helices* in the following) for achieving this goal.

The ubiquity of slender structures makes their digitalization a very active field of research in computer science. While digital curves are traditionally created from scratch by artists or designers [17, 28, 18, 6], more recent approaches alleviate this manual task by developing automatic capture processes based on photographs or magnetic resonance imaging data (MRI) [20, 16, 27, 24].

Once digitalized, slender structures are mostly represented as sequences of 3d points or as splines such as Bézier splines or non-uniform rational basis splines (NURBS). Both types of representations, particularly the sequences

2

of 3d points, require a large amount of storage space, especially when the curve exhibits an intricate shape. Furthermore, such representations do not offer direct information on the intrinsic properties of the curve, such as how the curve bends or twists.

In contrast, a G^1 piecewise helix can be described with only 3 parameters per element (length, curvature and torsion), thus offering a compact representation for a curve while providing direct information on how the curve bends or twists. Sloss [26] proved that it is possible to approximate a C^3-smooth curve with helices as closely as desired, which lets one think that helices could be a good candidate for compressing data, in a similar fashion to circular arcs [23]. Another interesting application would be curve animation, as G^1 piecewise helices could be easily plugged into the dynamic super-helix model introduced by Bertails et al. [3].

In this paper, we present a new, robust and fast algorithm to approximate a 3d curve with a G^1 piecewise helical curve. Our method is a full and non trivial 3d generalization of our 2d algorithm presented in [9] which addresses the particular case of a planar curve fitted by a piecewise circular arcs curve.

2. Related work

Existing approaches for approximating 3d curves by helices can be classified in 3 main categories: parameters identification, global optimization and local geometric interpolation methods.

Helix parameters identification. In the fields of biology and chemistry, many algorithms have been developed to fit helices to data, in order to analyse the 3d structure of DNA or proteins. These algorithms take as an input a sequence of 3d points describing a helix and return the parameters of the helix, namely its axis, radius and pitch. Christopher et al. [8] describe several methods to calculate the axis of the helix and then compare their speed and their robustness. To go further, Nievergelt [19] introduces a method to calculate both the axis of the helix and its radius at the same time by fitting a cylinder to the input points. As a second step of its algorithm, the author computes the pitch of the helix to complete the identification. Enkhbayar et al. [12] present a helix fitting method, *HELFIT*, that follows the general idea of [19], but adds an optimization of the parameters as a third step to improve the identification of the parameters.

Since those methods assume the input points to approximately lie on a helix, they are not robust enough for fitting helices to an arbitrary 3d curve with no prescribed geometry.

Global optimization. As shown by Sloss [26], it is possible to approximate a smooth curve with a piecewise helix as closely as desired. This means that given an arbitrary error ϵ, it is possible to find a piecewise helix such that the distance between the input curve and the piecewise helix lies below ϵ. Then, a natural way of approaching a curve with helices is to use a global optimization scheme. Piuze et al. [21] propose an optimization algorithm based on the Fréchet distance to fit generalized helicoids to 3d curves. The generalized helicoids can be obtained by making a twisted curve rotate around an axis while being displaced parallel to this axis. When the twisted curve is a straight line, then the trace generated by the helicoid is a helix. In their paper, the Nelder-Mead algorithm is used to minimize the Fréchet distance between the 3d curve and the trace generated by the generalized helicoid.

Other optimization approaches consist in minimizing the distance between the input curve and the piecewise helix with a least-squares optimization algorithm, e.g. the Levenberg-Marquardt algorithm used by Bergbom et al. [2]. We followed a similar strategy in [10] as a first attempt to approximate Bézier splines with G^1 piecewise helices, with a direct control over the number of elements.

Though natural, optimization-based approaches applied to our problem suffer from a high computational cost and lack of robustness. This is mainly due to the nonconvexity of the cost function resulting from the approximation of curves with helices.

Local geometric interpolation. The basic idea behind local geometric interpolation is to interpolate a discrete subset of points from the input 3d curve. Goriely et al. [14] introduce the *polyhelix*, a piecewise helix with a continuous Frenet frame, and present a method to interpolate a sequence of points with a polyhelix given the Frenet frame at the first point. Their idea is to find the shortest helix among those starting from the first point and ending at the second point. Then, the Frenet frame is propagated to the second point and the interpolation is applied to the second point and the third one, and so on. This approach implies the continuity of the Frenet frame for the piecewise helix. The resulting piecewise helix is then necessarily a G^2 curve, thus discarding all other G^1 interpolants. Moreover, this technique is very sensitive

Figure 2: Approximation of a 2d spline (in black) by a polycircle (in grey) with 13 circular arcs. As only points and the first (left) tangent are interpolated, an increasing drift of the approximation can be observed from left to right.

to the drift of the original Frenet frame, as we demonstrate in the 2d case (polycircle) in Figure 2. Therefore, interpolating only points of the input curve does not guarantee the quality of the approximation. In our work, we claim that accounting for the tangents helps preserve the global shape of the 3d curve. Unfortunately, it is well-known that in 2d, it is impossible to interpolate 2 points and 2 tangents with a single circular arc in the general case: points should lie on a line given by the tangents. Ghosh [13] generalized this assertion to 3d by stating that it is also impossible to interpolate 2 points along with their tangents using a single helix, unless points and tangents satisfy a particular configuration analogous to the 2d case.

Following the biarcs idea [4] for 2d interpolation, Ghosh [13] introduced the bihelices – a G^1 curve smoothly connecting 2 helices. bihelices allow for the interpolation of points along with their tangents in 3d by adding the locus of the joint point as a degree of freedom. However, given two points and two tangents, there is an infinite number of bihelices that interpolate those points and tangents. Finding the one that fits best the part of the curve in-between the two points requires an optimization scheme and thus may be computationally expensive. We especially showed in [9] that the biarcs method can be time consuming in 2d and one may expect the same issue with the bihelices method.

2d floating tangents. In [9], we proposed an alternative to the biarcs, based on the idea of interpolating the tangents *only*. As the problem of interpolating 2 points and 2 tangents with a single circular arc is over-constrained and since we believe that tangents are key descriptors for the global shape of a curve, we proposed to relax the constraint of going through the points, or, in other terms, to relax the points positions. In this hybrid approach, we

first perform a minimization of the displacement of the points, which boils down to the solving of a linear problem. Then, we interpolate the floating tangents using circular arcs, which is a trivial problem in 2d.

In this paper, we demonstrate that it is possible – though not trivial – to generalize the floating tangents method to the 3d case. Like in the 2d case, our method provides direct tuning of the number N of helical arcs used in the curve approximation, thus offering an intuitive control over the storage size used for the piecewise helix. A first pass then converts the input curve into a sequence of N points along with their tangents. Thanks to Ghosh's theorem which states the existence criterion of a helix with two fixed end points, we are able to safely and naturally extend our 2d points relaxation algorithm to the third dimension, coming up with a linear problem of size $2N + 3$ to be solved. By furthermore completing the proof of Ghosh's theorem, we derive a helix interpolation algorithm that remains valid in the general case. Our final approximation method turns out to be both fast and reliable, even when applied to complex input data stemming either from manual design or automatic image-based reconstruction.

3. Overview of the algorithm

Our algorithm closely approximates a Bézier spline with a G^1 piecewise helical curve, where the number of helical elements is given by the user. In other terms, our algorithm takes a Bézier spline as an input along with an integer N, and returns a G^1 piecewise helical curve composed of N helical arcs that approximates the Bézier curve.

Our algorithm proceeds in 3 main steps:

1. Cut the Bézier spline into N pieces of same length and compute the tangents at the break points.
2. Relax break points to satisfy the condition of interpolation found by Ghosh [13]. This step is described in Section 4.
3. Interpolate each pair of subsequent break points along with their tangents. The description of this step can be found in Section 5 along with a sketch of the complete proof of Ghosh's theorem (only partially proved in [13]). The detailed proof is given in Appendix A.

In Section 6, we present and analyze the results of our algorithm on a large range of data sets.

4. Points relaxation

The principle of *floating tangents* that we introduced in [9] in the 2d case can be extended to 3d, provided the local interpolation problem between a pair of points and tangents can be solved – what we shall see in Section 5. The general idea is to relax points $\mathbf{p}_0 \ldots \mathbf{p}_N$ to unknown positions $\mathbf{p}'_0 \ldots \mathbf{p}'_N$ so that each pair of new points $\mathbf{p}'_i, \mathbf{p}'_{i+1}$ along with their tangent vectors $\mathbf{t}'_i, \mathbf{t}'_{i+1}$ are co-helical – *i.e.*, a helix goes through $\mathbf{p}'_i$ and $\mathbf{p}'_{i+1}$ with $\mathbf{t}'_i$ and $\mathbf{t}'_{i+1}$ as respective tangents – and so that the new tangents $\mathbf{t}'_0 \ldots \mathbf{t}'_N$ match the old ones, that is $\forall i \in \{0, \ldots, N\}, \quad \mathbf{t}'_i = \mathbf{t}_i$. More precisely, we minimize the distance between the new points $\mathbf{p}'_i$ and the old ones $\mathbf{p}_i$. This can be expressed as a constrained least squares problem, as in 2d [9],

$$
\begin{array}{ll}
\min_{\{\mathbf{p}'_i\}_{i=0\ldots N}} & \sum_{i=0}^{N} ||\mathbf{p}'_i - \mathbf{p}_i||^2 \\
\text{subject to} & \text{(a)} \quad \mathbf{p}'_i, \ \mathbf{p}'_{i+1} \ \text{co-helical} \quad \forall i = 0 \ldots N-1 \\
& \text{(b)} \quad \mathbf{t}'_i = \mathbf{t}_i \quad \forall i = 0 \ldots N.
\end{array}
\tag{1}
$$

Co-helicity condition. In 2d, the condition of co-circularity of 2 points and 2 tangents is trivial. This is not the case in 3d. Ghosh [13] expressed the co-helicity condition through a simple and powerful theorem, stating that two points $\mathbf{p}_0$ and $\mathbf{p}_1$ along with their two tangent vectors $\mathbf{t}_0$ and $\mathbf{t}_1$ are co-helical if and only if

$$
\langle \mathbf{p}_1 - \mathbf{p}_0 \,, \, \mathbf{t}_1 - \mathbf{t}_0 \rangle = 0, .
\tag{2}
$$

where $\langle \mathbf{a} \,, \mathbf{b} \rangle$ denotes the inner product in $\mathbb{R}^3$ between vectors $\mathbf{a}$ and $\mathbf{b}$. Proving this statement is not straightforward and Ghosh's proof is only valid for some specific cases. In Section 5, we complete Ghosh's proof and present the interpolation algorithm in the general case.

Approximation with one helix. Geometrically, Equation (2) means that the two points $\mathbf{p}_0$ and $\mathbf{p}_1$ lie in a plane normal to the vector $\mathbf{t}_1 - \mathbf{t}_0$. In other terms, it means that the point $\mathbf{p}_1$ belongs to the plane normal to $\mathbf{t}_1 - \mathbf{t}_0$ which contains $\mathbf{p}_0$. This can be written as

$$
\mathbf{p}_1 = \mathbf{p}_0 + \alpha_0 \mathbf{v}_0 + \alpha_1 \mathbf{v}_1,
$$

with $(\mathbf{v}_0, \mathbf{v}_1)$ a basis of the vectorial plane normal to the vector $\mathbf{t}_1 - \mathbf{t}_0$ and α_0 and α_1 two real scalars. Denoting by $\mathbf{D}$ the matrix formed by the two

vectors $\mathbf{v}_0$ and $\mathbf{v}_1$,

$$\mathbf{D} = \begin{pmatrix} | & | \\ \mathbf{v}_0 & \mathbf{v}_1 \\ | & | \end{pmatrix}$$

and $\mathbf{a}$ the vector ${}^t(\alpha_0, \alpha_1)$, we get the linear relationship

$$\mathbf{p}_1 = \mathbf{p}_0 + \mathbf{D}\mathbf{a}. \tag{3}$$

It is noteworthy that Equation (3) is the same linear relationship as the one emerging in 2d from the co-circularity condition [9]. Therefore, the floating tangents algorithm in 3d can be derived in a similar fashion to the 2d algorithm.

Approximation with N helices. In the case of N helices, we have a set of $N+1$ points $\mathcal{P}$ along with their tangents $\mathcal{T}$ and we displace the points to new positions $\mathcal{P}'$ so that

$$\forall i \in \{0, \dots, N\}, \quad \langle \mathbf{p}'_{i+1} - \mathbf{p}'_i, \, \mathbf{t}_{i+1} - \mathbf{t}_i \rangle = 0. \tag{4}$$

Considering the $N+1$ tangent vectors $\mathbf{t}_0 \dots \mathbf{t}_N$, we can build N matrices

$$\mathbf{D}_i = \begin{pmatrix} | & | \\ \mathbf{v}_{0,i} & \mathbf{v}_{1,i} \\ | & | \end{pmatrix}$$

with $(\mathbf{v}_{0,i}, \mathbf{v}_{1,i})$ a basis of the vectorial plane normal to the vector $\mathbf{t}_{i+1} - \mathbf{t}_i$. Then, we have

$$\forall i \in \{0, \dots N-1\} \quad \mathbf{p}'_{i+1} = \mathbf{p}'_i + \mathbf{D}_i \mathbf{a}_i \text{ with } \mathbf{a}_i = \begin{pmatrix} \alpha_{0,i} \\ \alpha_{1,i} \end{pmatrix} \in \mathbb{R}^2.$$

Starting from $\mathbf{p}'_0$, we get

$$\mathbf{p}'_i = \mathbf{p}'_0 + \sum_{j=0}^{i-1} \mathbf{D}_j \mathbf{a}_j,$$

and finally, the constrained minimization problem (1) boils down to an unconstrained, convex quadratic problem

$$\min_{\mathcal{A}, \mathbf{p}'_0} \sum_{i=0}^{N} ||\mathbf{p}'_0 + \sum_{j=0}^{i-1} \mathbf{D}_j \mathbf{a}_j - \mathbf{p}_i||^2$$
$$= \min_{\mathcal{A}, \mathbf{p}'_0} F_{\mathcal{V}, \mathcal{P}}(\mathcal{A}, \mathbf{p}'_0),$$

with $\mathcal{A} = \{\alpha_{i,0}, \alpha_{i,1} \mid i \in [0, N-1]\}$ and $\mathcal{V} = \{\mathbf{v}_{i,0}, \mathbf{v}_{i,1} \mid i \in [0, N-1]\}$. This appears to be the same problem as in 2d, with a doubled set of variables. Solving it amounts to solving a linear system of $2N + 3$ equations,

$$\begin{cases} \frac{\partial F_{\mathcal{V}, \mathcal{P}}}{\partial \mathbf{p}'_{0x}} = 0 \\ \frac{\partial F_{\mathcal{V}, \mathcal{P}}}{\partial \mathbf{p}'_{0y}} = 0 \\ \frac{\partial F_{\mathcal{V}, \mathcal{P}}}{\partial \mathbf{p}'_{0z}} = 0 \\ \frac{\partial F_{\mathcal{V}, \mathcal{P}}}{\partial \alpha_{i,j}} = 0 \quad \forall i \in [0, N-1], \forall j \in \{0, 1\}. \end{cases} \quad (5)$$

Computing the partial derivatives appearing in (5) is straightforward and is left to the reader. The full algorithm of floating tangents is summed-up in Algorithm 1. In practice, we solve System (5) using a LU decomposition.

Algorithm 1 Floating tangents algorithm in 3d

Input: A sequence of N points $\mathcal{P}$ and a sequence of N tangents $\mathcal{T}$
Output: A sequence of N points $\mathcal{P}'$ satisfying (4)
  for $i \leftarrow 0$ to $N - 1$ **do**
    Compute $\mathbf{v}_{i,0}$ and $\mathbf{v}_{i,1}$
  end for
  Compute the derivatives appearing in (5)
  Solve System (5) for $\mathcal{A}$ and $\mathbf{p}'_0$
  for $i \leftarrow 0$ to $N - 1$ **do**
    Compute $\mathbf{p}'_{i+1}$ with $\mathbf{p}'_{i+1} = \mathbf{p}'_i + \alpha_{i,0}\mathbf{v}_{i,0} + \alpha_{i,1}\mathbf{v}_{i,1}$
  end for

---

5. Points and tangents interpolation

In this section, we address the problem of interpolating two points along with two tangents using a single helix. More precisely, we base our algorithm on the theorem provided by Ghosh [13]:

Theorem 5.1. *Given two points $\boldsymbol{p}_0$ and $\boldsymbol{p}_1$ such that $\boldsymbol{p}_0 \neq \boldsymbol{p}_1$ and two tangents $\boldsymbol{t}_0$ and $\boldsymbol{t}_1$ such that $\boldsymbol{t}_1 \neq \pm\boldsymbol{t}_0$, there exists a unique short helix (see Definition 5.1) starting at $\boldsymbol{p}_0$ with tangent $\boldsymbol{t}_0$ and ending at $\boldsymbol{p}_1$ with tangent $\boldsymbol{t}_1$ if and only if*

$$\langle \boldsymbol{p}_1 - \boldsymbol{p}_0 \,,\, \boldsymbol{t}_1 - \boldsymbol{t}_0 \rangle = 0. \tag{6}$$

In Ghosh's thesis, only the uniqueness of such a helix is proved, furthermore limited to a subspace of solutions. Here however, we need to prove that our interpolation algorithm works in the *general* case. In the following, we sketch the main steps of our generalized proof, which builds on Ghosh's initial proof, adapts it, and extends it so as to fulfill our needs. The reader may find the full proof along with technical details in Appendix A.

5.1. Equation of a helix and definition of a short helix

Following Ghosh, we start by describing a helix $\boldsymbol{\alpha}$ and its tangent $\mathbf{t}$ in an adapted frame. This frame is built from the tangent $\mathbf{t}_0$ at the starting point (of arc length 0) and from the Darboux vector $\boldsymbol{\Omega}$ of the helix. Note that in the particular case of helices, $\boldsymbol{\Omega}$ is uniform and parallel to the axis of the helix. Unlike Ghosh, we use the traditional convention of the Darboux vector (given in Equation (A.3)), which yields the following equations,

$$\boldsymbol{\alpha}(s) = \mathbf{p}_0 + \bar{\tau}s\bar{\boldsymbol{\Omega}} + C(s)(\mathbf{t}_0 - \bar{\tau}\bar{\boldsymbol{\Omega}}) - S(s)(\mathbf{t}_0 \times \bar{\boldsymbol{\Omega}}) \tag{7}$$
$$\mathbf{t}(s) = \mathbf{t}_0 + (\cos\omega s - 1)(\mathbf{t}_0 - \bar{\tau}\bar{\boldsymbol{\Omega}}) - \sin\omega s(\mathbf{t}_0 \times \bar{\boldsymbol{\Omega}}),$$

with $\mathbf{p}_0$ the starting point of the helix and $\mathbf{t}_0$ its tangent. The geometry of the helix is described by its Darboux vector $\boldsymbol{\Omega}$, with ω its length, $\bar{\boldsymbol{\Omega}}$ the normalized vector $\bar{\boldsymbol{\Omega}} = \frac{1}{\omega}\boldsymbol{\Omega}$, and τ its torsion with $\bar{\tau} = \frac{\tau}{\omega}$. The curvature of the helix can be obtained by $\kappa = \sqrt{\omega^2 - \tau^2}$. Finally, two functions C and S are defined as

$$C(s) = \frac{\sin\omega s}{\omega},$$
$$S(s) = \frac{1 - \cos\omega s}{\omega}.$$

10

With the change of variable $\varphi = \omega s$, φ being the azimuthal angle (see Figure 3), we get

$$\boldsymbol{\alpha}(\varphi) = \mathbf{p}_0 + \bar{\tau}\frac{\varphi}{\omega}\bar{\boldsymbol{\Omega}} + \frac{\sin\varphi}{\omega}(\mathbf{t}_0 - \bar{\tau}\bar{\boldsymbol{\Omega}})$$
$$- \frac{1 - \cos\varphi}{\omega}(\mathbf{t}_0 \times \bar{\boldsymbol{\Omega}}),$$
$$\mathbf{t}(\varphi) = \mathbf{t}_0 + (\cos\varphi - 1)(\mathbf{t}_0 - \bar{\tau}\bar{\boldsymbol{\Omega}}) - \sin\varphi(\mathbf{t}_0 \times \bar{\boldsymbol{\Omega}}).$$

The details on how to obtain those equations can be found in Appendix A. We now define a *short helix* similarly as in [13]:

Definition 5.1. *A helix of axis $\bar{\boldsymbol{\Omega}}$ is called a short helix when its projection onto the plane orthogonal to $\bar{\boldsymbol{\Omega}}$ is a circle arc that is not a full circle.*

Considering Equation (7), the projection of the helix onto the plane orthogonal to $\bar{\boldsymbol{\Omega}}$ reads

$$\boldsymbol{\alpha}_{\perp}(\varphi) = \mathbf{p}_0 + \frac{\sin\varphi}{\omega}(\mathbf{t}_0 - \bar{\tau}\bar{\boldsymbol{\Omega}}) - \frac{1 - \cos\varphi}{\omega}(\mathbf{t}_0 \times \bar{\boldsymbol{\Omega}})$$

which is the equation of a circle. Defining φ_* such that $\varphi_* = \omega l$, where l is the length of the helix, this curve is a short circle arc when we have (see Figure 3)

$$\varphi_* \in [0, 2\pi[.$$

5.2. Proof of the theorem

Proving that Condition (6) is necessary is straightforward and is achieved in Appendix A. Proving that this condition is sufficient requires more calculations. We need to prove that if

$$\langle \mathbf{p}_1 - \mathbf{p}_0, \, \mathbf{t}_1 - \mathbf{t}_0 \rangle = 0,$$

then there exists a unique short helix interpolating the points $\mathbf{p}_0$ and $\mathbf{p}_1$ and the tangents $\mathbf{t}_0$ and $\mathbf{t}_1$ (see Figure 3). We proceed with an analysis-synthesis reasoning.
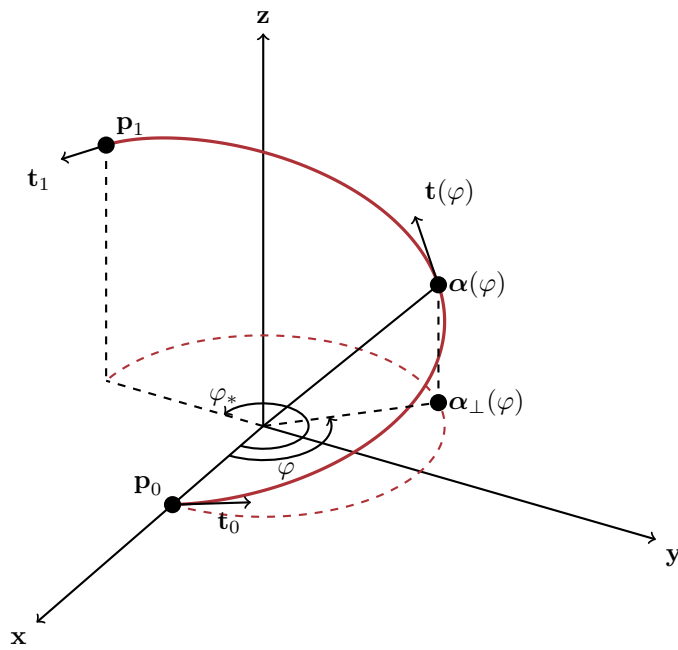
Figure 3: The unique short helix that interpolates $\mathbf{p}_0$ and $\mathbf{p}_1$ with tangents $\mathbf{t}_0$ and $\mathbf{t}_1$ when Eq. (6) is satisfied.

- **Analysis:** We assume that such a helix exists and we precisely characterize its parameters $\bar{\boldsymbol{\Omega}}$, ω, $\bar{\tau}$ and φ_* so that we can conclude that this helix is unique. This first part was addressed by Ghosh, with a partial characterization of the parameter φ_*. We fully characterize φ_* in Section 5.2.1.

- **Synthesis:** We consider the helix with the parameters we found in the analysis to prove that it interpolates the two points and the two tangents, proving the existence of the helix. This second part was not addressed in Ghosh's proof and we present it in Appendix A.

For the rest of the proof, we consider two points $\mathbf{p}_0$ and $\mathbf{p}_1$ and two unit vectors $\mathbf{t}_0$ and $\mathbf{t}_1$ satisfying Condition (6). Following Ghosh's proof, let us define
$$t_0 = \langle \mathbf{t}_0 \, , \, \mathbf{t}_1 \rangle$$
and let us assume that $\mathbf{t}_1 \neq \pm \mathbf{t}_0$, so that

$$t_0 \in \,]{-1} \, ; \, 1[\, .$$

5.2.1. Condition (6) is sufficient: analysis

In the analysis, we follow the steps of Ghosh's proof, and particularly the key idea of the whole proof, which is to cleverly write the equations of the helix and its tangent in a well-chosen basis of $\mathbb{R}^3$. The main difference with Ghosh's proof here is that we fully characterize parameter φ_*.

Let us assume the existence of a short helix $\mathscr{H}$ parametrized by arclength, which interpolates points $\mathbf{p}_0$ and $\mathbf{p}_1$ with $\mathbf{t}_0$ and $\mathbf{t}_1$ as respective tangents. We have then

$$\begin{aligned}
\mathbf{p}_1 = \boldsymbol{\alpha}(\varphi_*) &= \mathbf{p}_0 + \bar{\tau}\frac{\varphi_*}{\omega}\bar{\boldsymbol{\Omega}} + \frac{\sin\varphi_*}{\omega}(\mathbf{t}_0 - \bar{\tau}\bar{\boldsymbol{\Omega}}) \\
&\quad - \frac{1-\cos\varphi_*}{\omega}(\mathbf{t}_0 \times \bar{\boldsymbol{\Omega}}), \\
\mathbf{t}_1 = \mathbf{t}(\varphi_*) &= \mathbf{t}_0 + (\cos\varphi_* - 1)(\mathbf{t}_0 - \bar{\tau}\bar{\boldsymbol{\Omega}}) - \sin\varphi_*(\mathbf{t}_0 \times \bar{\boldsymbol{\Omega}}).
\end{aligned} \tag{8}$$

Writing these two equations in the orthonormal basis $(\mathbf{e}_1, \mathbf{e}_2, \mathbf{e}_3)$ introduced by Ghosh as

$$\mathbf{e}_1 = \frac{1}{\sqrt{2(1+t_0)}}(\mathbf{t}_1 + \mathbf{t}_0),$$

$$\mathbf{e}_2 = \frac{1}{\sqrt{1-t_0^2}}(\mathbf{t}_1 \times \mathbf{t}_0),$$

$$\mathbf{e}_3 = \frac{1}{\sqrt{2(1-t_0)}}(\mathbf{t}_1 - \mathbf{t}_0),$$

we obtain the following lemma

Lemma 5.2. *Helix $\mathscr{H}$ with parameters ω, $\bar{\tau}$, φ_* and $\bar{\Omega}$ interpolates points $\boldsymbol{p}_0$ and $\boldsymbol{p}_1$ with respective tangents $\boldsymbol{t}_0$ and $\boldsymbol{t}_1$ such that $\boldsymbol{t}_1 \neq \pm \boldsymbol{t}_0$ if and only if*

$$\begin{cases} \omega \, |\langle \boldsymbol{p}_1 - \boldsymbol{p}_0 \,,\, \boldsymbol{t}_1 \times \boldsymbol{t}_0 \rangle| = -\frac{\sqrt{2}(1-t_0)}{1-\cos\varphi_*} D(\varphi_*), \\[2mm] \omega \, \langle \boldsymbol{p}_1 - \boldsymbol{p}_0 \,,\, \boldsymbol{t}_1 + \boldsymbol{t}_0 \rangle = \frac{2}{1-\cos\varphi_*} N(\varphi_*), \\[2mm] \bar{\tau} = \text{sign}\langle \boldsymbol{p}_1 - \boldsymbol{p}_0 \,,\, \boldsymbol{t}_1 \times \boldsymbol{t}_0 \rangle \sqrt{\dfrac{t_0 - \cos\varphi_*}{1 - \cos\varphi_*}}, \\[2mm] \bar{\Omega} = \frac{1}{1+t_0}\left(\bar{\tau}(\boldsymbol{t}_1 + \boldsymbol{t}_0) + \left(\cot\frac{\varphi_*}{2}\right)(\boldsymbol{t}_1 \times \boldsymbol{t}_0)\right), \\[2mm] \varphi_* \in I_0, \end{cases} \tag{9}$$

with

$$N(\varphi) = (1-t_0)\sin\varphi + \varphi(t_0 - \cos\varphi),$$
$$D(\varphi) = (\varphi\cos\tfrac{\varphi}{2} - 2\sin\tfrac{\varphi}{2})\sqrt{t_0 - \cos\varphi},$$
$$I_0 = [\arccos t_0, 2\pi - \arccos t_0] \quad with \quad t_0 = \langle \boldsymbol{t}_0 \,,\, \boldsymbol{t}_1 \rangle \in \,]{-1}\,;1[\,.$$

This lemma (proved in Appendix A) is relevant since it provides an equivalence that we shall be exploiting in the synthesis part 5.2.2 to prove that a helix $\mathscr{H}$ with parameters ω, $\bar{\tau}$, φ_* and $\bar{\Omega}$ indeed interpolates the two points and two tangents when its parameters satisfy Equation (9). Moreover, once φ_* and ω are assumed to be unique, this theorem gives a characterization of parameters $\bar{\tau}$ and $\bar{\Omega}$. The theorem is however not sufficient for proving the uniqueness of φ_* and ω, and we now explain how to achieve this. Considering

$$\langle \mathbf{p}_1 - \mathbf{p}_0 \,,\, \mathbf{p}_1 - \mathbf{p}_0 \rangle = \langle \boldsymbol{\alpha}(\varphi_*) - \mathbf{p}_0 \,,\, \boldsymbol{\alpha}(\varphi_*) - \mathbf{p}_0 \rangle,$$

14

we get, from (8)

$$\omega = \frac{\sqrt{2(1 - t_0) + (\bar{\tau}\varphi_*)^2}}{||\mathbf{p}_1 - \mathbf{p}_0||}.$$

To characterize φ_*, we need to consider N and D and particularly the values of φ where D vanishes. In Appendix A, we show that if

$$\langle \mathbf{p}_1 - \mathbf{p}_0, \, \mathbf{t}_1 \times \mathbf{t}_0 \rangle = 0,$$

then

$$D(\varphi_*) = 0$$

and

$$\varphi_* = \begin{cases} \arccos t_0 & \text{if } \langle \mathbf{p}_1 - \mathbf{p}_0, \, \mathbf{t}_1 + \mathbf{t}_0 \rangle < 0 \\ 2\pi - \arccos t_0 & \text{if } \langle \mathbf{p}_1 - \mathbf{p}_0, \, \mathbf{t}_1 + \mathbf{t}_0 \rangle > 0. \end{cases}$$

In the other case, where

$$\langle \mathbf{p}_1 - \mathbf{p}_0, \, \mathbf{t}_1 \times \mathbf{t}_0 \rangle \neq 0,$$

we define function H as

$$H(\varphi_*) = \frac{N(\varphi_*)}{D(\varphi_*)} = -\chi \tag{10}$$

with

$$\chi = \frac{(1 - t_0)\langle \mathbf{p}_1 - \mathbf{p}_0, \, \mathbf{t}_1 + \mathbf{t}_0 \rangle}{\sqrt{2} \times |\langle \mathbf{p}_1 - \mathbf{p}_0, \, \mathbf{t}_1 \times \mathbf{t}_0 \rangle|}$$

which is a well-defined constant that only depends on $\mathbf{p}_0$, $\mathbf{p}_1$, $\mathbf{t}_0$ and $\mathbf{t}_1$.

We now prove that the following equation,

$$H(\varphi_*) = -\chi \tag{11}$$

has a unique solution. Ghosh restricted the domain of solutions to the interval

$$I_G = [\arccos t_0, \pi] \subsetneq I_0,$$

where I_0 is defined in Equation (9). We complete the study of H to the interval I_0. Thus, we prove that φ_* is unique, as well as all the parameters of the helix $\mathscr{H}$. Therefore, we conclude that helix $\mathscr{H}$ is unique which completes the analysis.

To prove that Equation (11) has a unique solution over I_0, we first notice that

$$\lim_{\varphi \to \arccos t_0^+} H(\varphi) = -\infty$$
$$\lim_{\varphi \to 2\pi - \arccos t_0^-} H(\varphi) = +\infty.$$

Since it is easy to see that H is a continuous function, we conclude that a solution to Equation (11) exists. To prove uniqueness, we show that H is strictly increasing over I_0. More precisely, we show that its derivative is strictly positive over I_0. We have, for all t_0 and all φ

$$H'(\varphi) = -\frac{(1 + t_0)\sin\frac{\varphi}{2}}{2D^2(\varphi)\sqrt{t_0 - \cos\varphi}}(h_0(\varphi)t_0 + h_1(\varphi)),$$

with

$$h_0(\varphi) = 4 - \varphi^2 - 4\cos\varphi - \varphi\sin\varphi$$
$$h_1(\varphi) = -1 + \cos 2\varphi + \varphi\sin\varphi + \varphi^2\cos\varphi.$$

It is easy to prove that

$$-\frac{(1 + t_0)\sin\frac{\varphi}{2}}{2D^2(\varphi)\sqrt{t_0 - \cos\varphi}} < 0,$$

meaning that we only need to study the sign of

$$h_0(\varphi)t + h_1(\varphi).$$

Let us define and study the two variable function

$$F(t, \varphi) = h_0(\varphi)t + h_1(\varphi)$$

on the closed domain

$$\mathcal{E} = \left\{ (t, \varphi), \begin{array}{l} t \in [-1, 1] \\ \varphi \in [\arccos t, 2\pi - \arccos t] \end{array} \right\}.$$
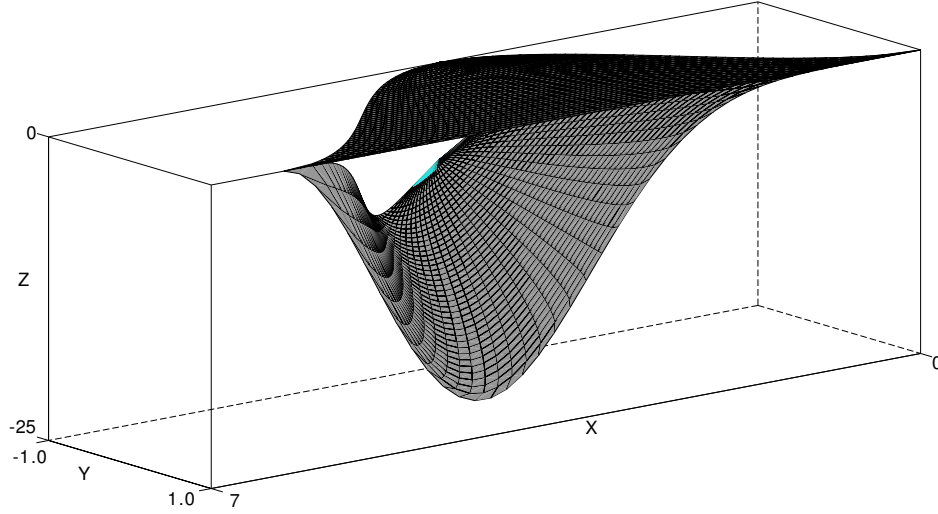
Figure 4: Representation of function F (in light grey) and space $\mathcal{E}$ (in dark grey). Note that $\mathcal{E}$ is a subset of $\mathbb{R}^2$, and is represented at height $z = 0$. This graph illustrates that over $\mathcal{E}$, F is always nonpositive.

The space $\mathcal{E}$ is closed and bounded since we have

$$\mathcal{E} = f^{-1}(]-\infty, 0]) \cap ([-1, 1] \times [0, 2\pi])$$

where f, such that

$$f(t, \varphi) = \cos \varphi - t,$$

is a continuous function on $\mathbb{R}^2$.

Therefore, since F is also continuous, F attains its maximum over $\mathcal{E}$. Particularly, its maximum is either in the interior or on the boundary of $\mathcal{E}$. If it is in the interior of $\mathcal{E}$, then the derivative of F vanishes at this point (it is a critical point). In Appendix A, we show that ∇F cannot vanish in the interior of $\mathcal{E}$. Thus, we deduce that F attains its maximum on the boundary

17

of $\mathcal{E}$. By denoting $\partial\mathcal{E} = \mathcal{F}_1 \cup \mathcal{F}_2 \cup \mathcal{F}_3 \cup \mathcal{F}_4$ the boundary of $\mathcal{E}$, with

$$\mathcal{F}_1 = \left\{ (t, \varphi), \begin{array}{l} t \in [-1, 1] \\ \varphi = \arccos t \end{array} \right\}$$

$$\mathcal{F}_2 = \left\{ (t, \varphi), \begin{array}{l} t \in [-1, 1] \\ \varphi = 2\pi - \arccos t \end{array} \right\}$$

$$\mathcal{F}_3 = \left\{ (t, \varphi), \begin{array}{l} t = -1 \\ \varphi \in [\pi, \pi] \end{array} \right\}$$

$$\mathcal{F}_4 = \left\{ (t, \varphi), \begin{array}{l} t = 1 \\ \varphi \in [0, 2\pi] \end{array} \right\}$$

we now study F over the 4 spaces $\mathcal{F}_1$, $\mathcal{F}_2$, $\mathcal{F}_3$ and $\mathcal{F}_4$. In Appendix A, we prove that over those spaces, the maximum value of F is equal to 0 and is only attained when

$$t_0 = 1.$$

Therefore, we conclude that F is negative over $\mathcal{E}$ (see 4 for a graphical illustration), and even that H' is strictly positive over I_0 and for all $t_0 \in]-1, 1[$. Thus, we conclude that Equation (11) has a unique solution over I_0.

From this analysis, we can extract an algorithm to interpolate two points and two tangents with a short helix, assuming that they satisfy Ghosh's condition of Theorem 5.1. This algorithm is presented in Section 5.3.

5.2.2. Condition (6) is sufficient: synthesis

The idea of the synthesis is to consider a helix with parameters ω, $\bar{\tau}$, φ_* and $\bar{\Omega}$ that satisfies the characterizations we obtained in the analysis above and to show that these parameters satisfy condition (9) of Theorem 5.2. All the details of the synthesis are presented in Appendix A.

5.3. Interpolation algorithm

The resulting interpolation method is derived in Algorithm 2. A similar algorithm is presented in Ghosh's thesis [13], however limited to the restriction I_G on the domain of φ_*. In practice, finding the unique root of $H(\varphi_*) + \chi$ can be simply and efficiently achieved through bisection.

Algorithm 2 Interpolation algorithm

Input: 2 points $\mathbf{p}_0$ and $\mathbf{p}_1$ and 2 tangents $\mathbf{t}_0$ and $\mathbf{t}_1$ with $\langle \mathbf{p}_1 - \mathbf{p}_0\,, \mathbf{t}_1 - \mathbf{t}_0 \rangle = 0$
Output: The unique short helix interpolating the two points and the two
    tangents

    Compute $t_0 \leftarrow \langle \mathbf{t}_0\,, \mathbf{t}_1 \rangle$
    Compute $\chi = \frac{(1-t_0)\langle \mathbf{p}_1 - \mathbf{p}_0\,, \mathbf{t}_1 + \mathbf{t}_0 \rangle}{\sqrt{2}|\langle \mathbf{p}_1 - \mathbf{p}_0\,, \mathbf{t}_1 \times \mathbf{t}_0 \rangle|}$
    Solve equation $H(\varphi_*) = -\chi$ with H given by (10)
    Compute $\bar{\tau} = \mathrm{sign}\langle \mathbf{p}_1 - \mathbf{p}_0\,, \mathbf{t}_1 \times \mathbf{t}_0 \rangle \sqrt{\frac{t_0 - \cos\varphi_*}{1 - \cos\varphi_*}}$
    Compute $\omega = \frac{\sqrt{2(1-t_0) + (\bar{\tau}\varphi_*)^2}}{\|\mathbf{p}_1 - \mathbf{p}_0\|}$
    Compute $\bar{\boldsymbol{\Omega}} = \frac{1}{1+t_0}\left(\bar{\tau}(\mathbf{t}_1 + \mathbf{t}_0) + \left(\cot\frac{\varphi_*}{2}\right)(\mathbf{t}_1 \times \mathbf{t}_0) \right)$
    return the helix of parameters $\bar{\boldsymbol{\Omega}}$, ω, $\bar{\tau}$ and φ_*
---

6. Evaluation and results

In this section, we present and evaluate the results of our floating tangents algorithm applied to various data sets, either synthetic or exported from captures of real data. We especially compare our method to a standard optimization based method used e.g. in [10] in terms of quality and computation time. As mentioned earlier, we showed in [9] that the biarcs method is accurate but can be time consuming in 2d. We thus expect the bihelices method introduced by Ghosh [13] to be even more time consuming in 3d. Furthermore, to our knowledge, such a method has not been evaluated so far for the fitting of arbitrary curves with helices. For all these reasons, we chose not to compare our algorithm with the bihelices method in this paper.

Finally, we show how our method robustly and efficiently scales to large and complex datasets coming from various sources ranging from biological to astrophysical data.

6.1. Framework for comparison

6.1.1. Measure of quality

We evaluate the quality of our approximation by comparing the resulting G^1 piecewise helix against the input Bézier spline, using the Fréchet distance [1]. Unlike the L_2 norm, the Fréchet distance adequately measures similarities between two curves. Indeed, the Fréchet distance between one curve and a slightly shifted version of it conveniently remains small, whereas

the L_2 distance may become unreasonably large. We implemented the discrete Fréchet distance algorithm introduced by Eiter and Mannila [11].

6.1.2. Algorithms to be compared

In the following results, we compare our floating tangents method against a natural optimization-based method that we formerly presented in [10]. In this optimization method, we sample the input Bézier spline and a piecewise helix given as a first iterate. Then the Levenberg-Marquardt least-squares algorithm is applied on the two sampled curves in order to fit the approximation to the input spline. The first iterate is set as the spline resulting from a piecewise constant approximation of the curvature-torsion of the input spline evenly cut into N pieces.

We tested several others configurations for the first iterate but experimentally found that the convergence of the algorithm was actually not influenced by the geometry of the first iterate.

6.1.3. Datasets used for comparison

We applied the two algorithms on 3 datasets (A, B, and C) created by an artist. Each one of those datasets contains around 240 Bézier splines measuring around 30 cm. They are represented in Figure 6.

6.1.4. Complexity of a curve

It is natural to think that the more straight and regular a curve is, the easier it will be to approximate. We define the complexity of a curve Γ as a new criterion to categorize curves, measured by the following quantity:

$$C(\Gamma) = \int_\Gamma \sqrt{\kappa^2 + \tau^2}. \tag{12}$$

With this definition, the more curved and twisted a curve is, the more complex it is. In Figure 5, we show the distribution of the complexity of the curves contained in the three datasets mentioned above. It confirms the visual impression given by Figure 6, that the curves in dataset C are more complex than the curves in dataset B which are themselves more complex than the curves in dataset A.

6.2. Quality of the approximation

In Figure 6, we present the results we obtained with both methods applied to the three datasets with $N = 15$ helical elements. The quality of the
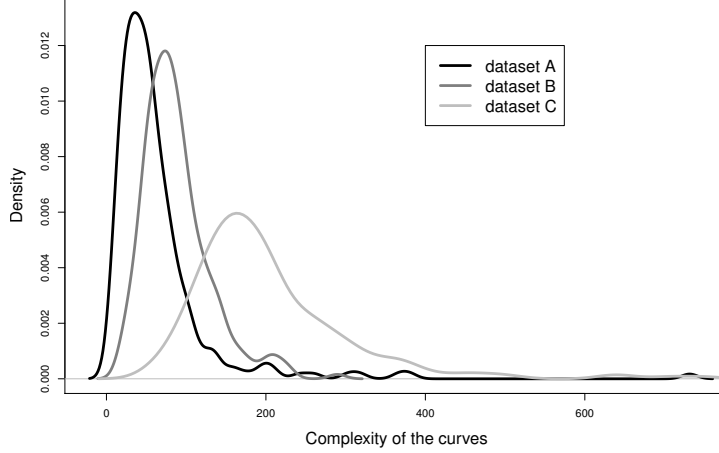
Figure 5: Distribution of the complexity of the curves from the 3 datasets, based on our complexity criterion defined in (12).

approximation appears to be better with our floating tangents method than with the optimization method, especially as the average complexity of the curves increases.

In Figure 7, we present the evolution of the average quality of the approximation with respect to the number of helical elements of the output curve for both algorithms applied to the three datasets. For both algorithms, the mean distance between the result of the approximation and the input spline decreases as the number of helical elements increases. Thus, the user can expect the quality of the approximation to improve as the number of helical elements increases. Note however that the average quality of the floating tangent method becomes higher compared to the optimization algorithm when the number of elements increases.

6.3. Computation time

We display in Figure 8 the computation time of both algorithms with respect to the complexity of the input curve when the algorithms are applied to the 3 datasets with $N = 10$ and $N = 15$ helical elements. Timings were measured on a single threaded application running on an Intel Xeon W3520 CPU at 2.67 GHz. Note that the computation time of our algorithm remains steady when the complexity of the curve increases. In contrast, the computation time of the optimization-based algorithm is more difficult
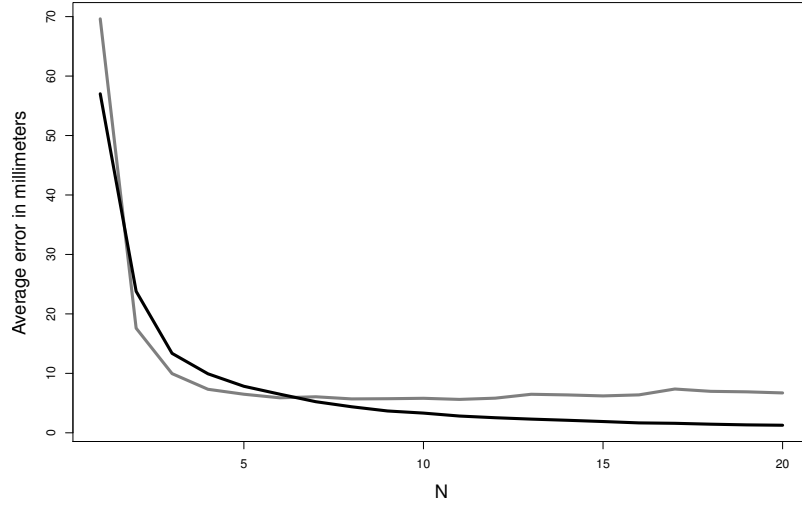
21
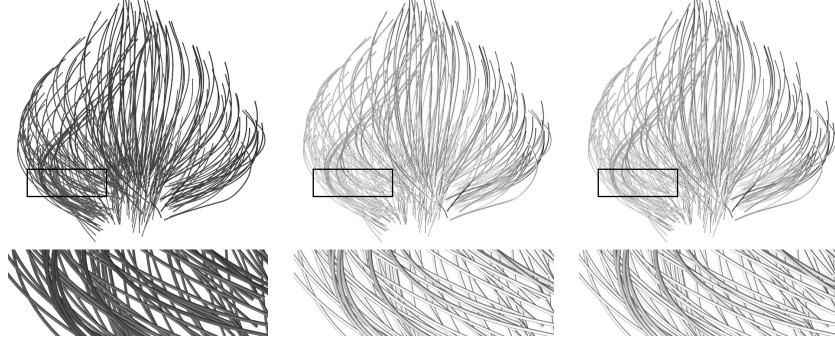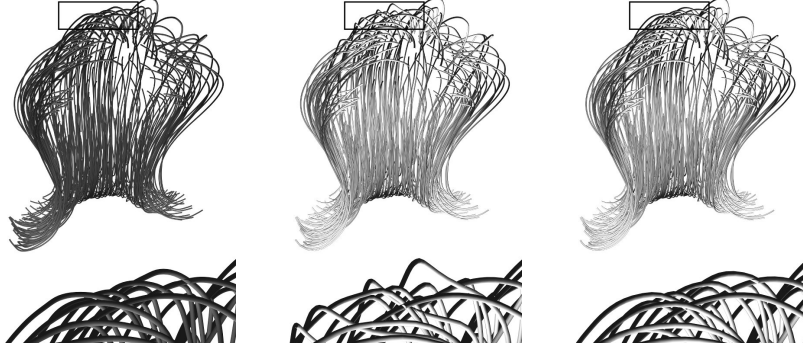
(a) Dataset A

(b) Dataset B

(c) Dataset C

Figure 6: The 3 datasets A, B, and C (left, in black) and the approximation results in grey, either produced by the optimization method (middle), or by our floating tangents method (right), both with $N = 15$ helical elements.

(a) Quality comparison between our floating tangents method (in black) and the optimization based method (in grey) measured with the Fréchet distance between the result of the approximation and the input curve, function of the number of helical elements.
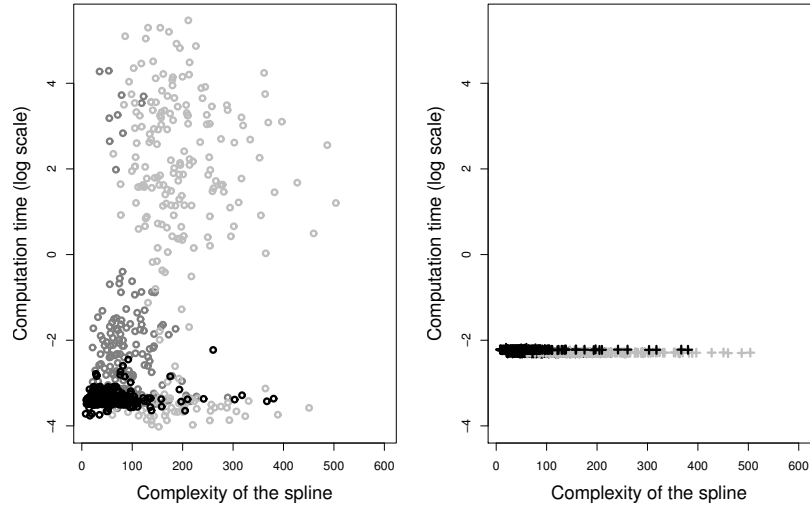
		Optimization	**Floating Tangents**
$N = 10$	ave. dist.	5.8	**3.3**
	max. dist.	44	**31**
$N = 15$	ave. dist.	6.2	**1.9**
	max. dist.	74	**12**

(b) Average and maximum Fréchet distance, measured in millimeters, for both algorithms applied to the 3 datasets, with 10 and 15 elements.

Figure 7: Quality measurement for both algorithms applied to the 3 datasets A, B, and C depicted in Figure 6.
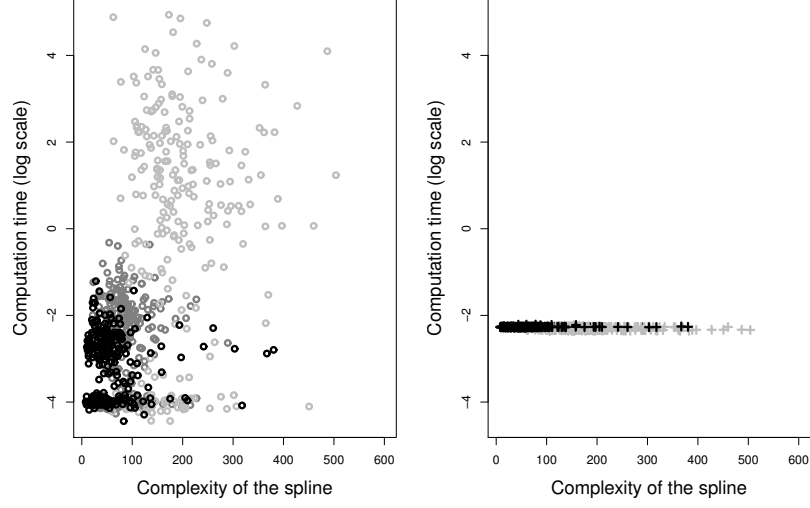
(a) $N = 10$

(b) $N = 15$

Figure 8: Computation time (expressed in seconds and in log space) of our floating tangents method (right) compared to the optimization based method (left), applied to the 3 datasets, A in black, B in dark grey and C in light grey, with respect to the complexity of the input curve. Note that, unlike the optimization based algorithm, our floating tangents method is not sensitive to the complexity of the input curve.

		Dataset A	Dataset B	DatasetC
$N = 10$	Optimization	13	27.8	2246
	Floating Tangents	**24.9**	**24.9**	**23.6**
$N = 15$	Optimization	8.7	370	4358
	Floating Tangents	**26**	**24.3**	**24**

Table 1: Total computation time in seconds of our method compared to the optimization-based approach, both applied to the 3 datasets A, B, and C, with $N = 10$ and $N = 15$ helical elements per approximation.

to predict as the complexity of the curve increases, as shown in Table 1, where we present the total computation time of both methods. The user can expect our algorithm to run at a constant speed, whatever the complexity of the input curve is, because our floating tangents method works regardless of the geometry of the input curve in-between the points we relax. This is not true with the optimization based algorithm since performance of the optimizer heavily depends on the geometry of the input curve.

To summarize, the floating tangents method appears to be a more reliable algorithm than the natural optimization based algorithm, both regarding the quality of the approximation and the computation time.

6.4. Large datasets

In the previous section, we have tested our method on a few synthetic datasets and showed that our algorithm was fast and accurate. Now, we apply our floating tangents method to a few challenging datasets captured from real world applications, coming from different sources [16, 22, 5], and presented in Figures 9, 10 and 11. The datasets respectively represent hair strands, heart muscular fibers and magnetic field lines of a star.

The curves contained in these datasets are stored sequences of 3d points. In order to apply our algorithm to these datasets, we had to convert the sequences of 3d points into Bézier splines. We achieved this by applying a 3d version of the curve smoothing algorithm used in Inkscape [15]. This algorithm is described in its 2d version in [25].
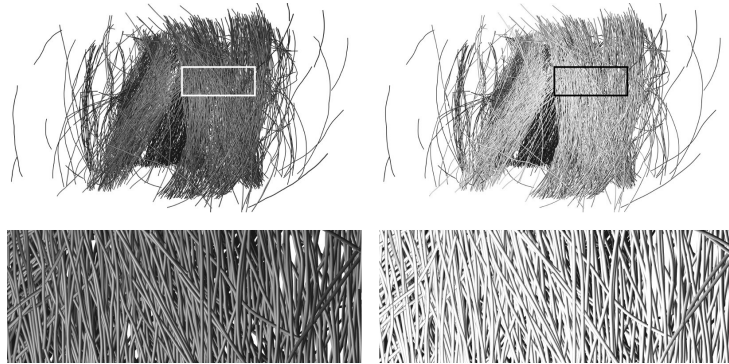
Note that due to the heterogeneity of the curves lengths in these datasets, we had to adapt the number of helical elements per curve depending on the length of each input curve. More precisely, we used 5 to 20 elements for the first 3 hair datasets of Figure 9, 2 to 100 elements for the heart muscular
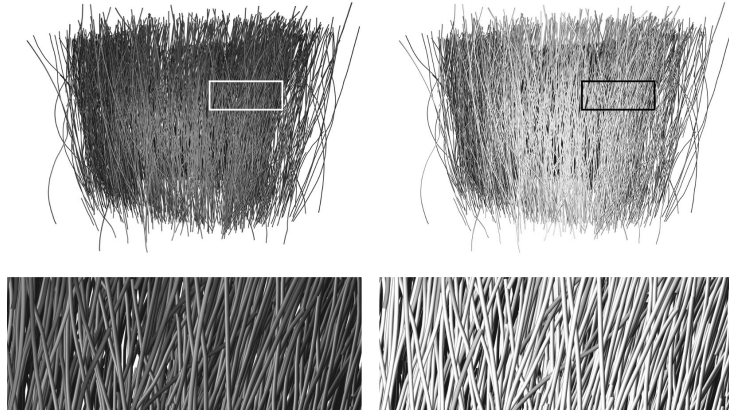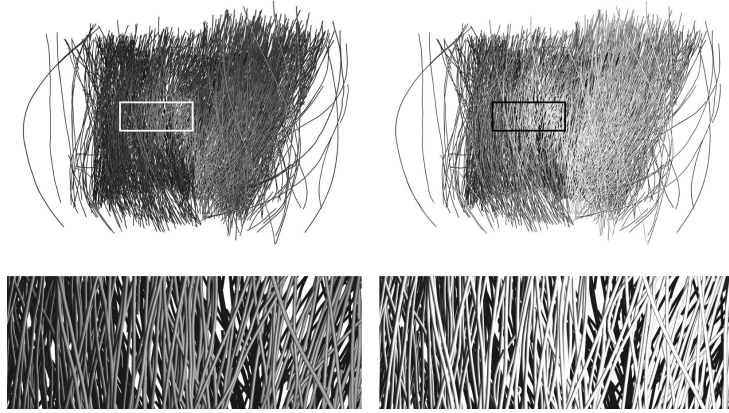
Figure 9: Our algorithm (right) applied to hair captures (around 2000 curves) from [16] (left).
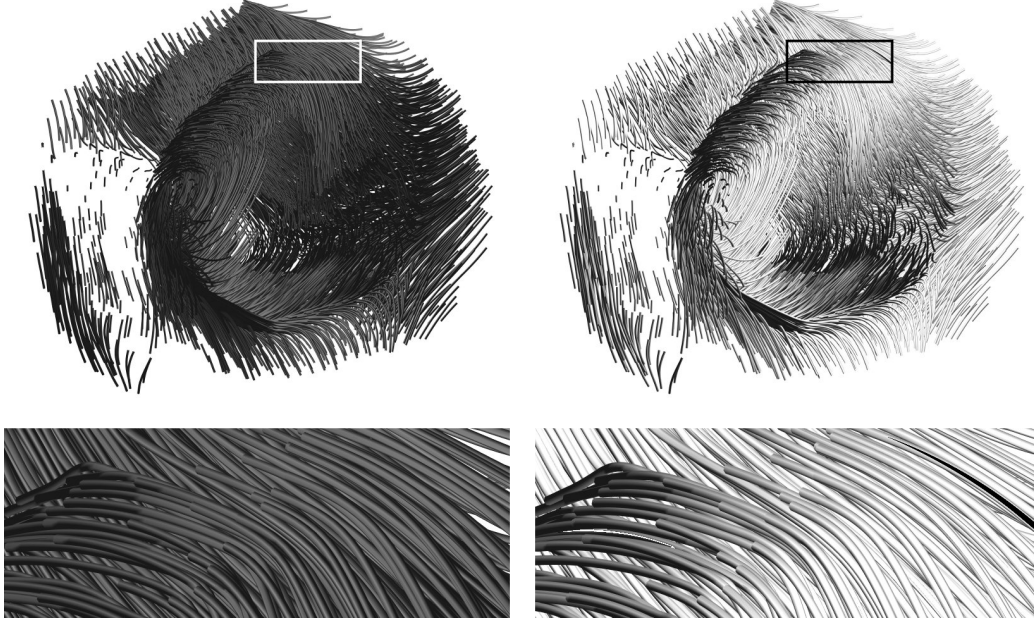
Figure 10: Our algorithm (right) applied to heart muscular fibers (around 3000 curves) from [22].

fibers dataset of Figure 10 and 2 to 200 elements for the magnetic lines dataset of Figure 11.

As shown in Table 2, the quality of the results is very satisfactory as the approximation always remains very close to the input curves, whatever the data set tested. Computational time keeps reasonable for all data sets, even for the complex magnetic fields lines composed of nine thousands lengthy and intricate curves, which only requires one hour to be fully processed. These successful tests show that our method scales well to real and challenging datasets.

6.5. Discussion and limitations

In Table 3, we present the computation time of the different parts of the algorithm. It is noticeable that most of the time is spent in the spline sampling part. This means that the floating tangent method remains very fast on real datasets, requiring time mostly for the spline sampling. In our present work we did not focus on optimizing this preprocessing step and thus we believe there is still room for some improvements including some gain in speed.
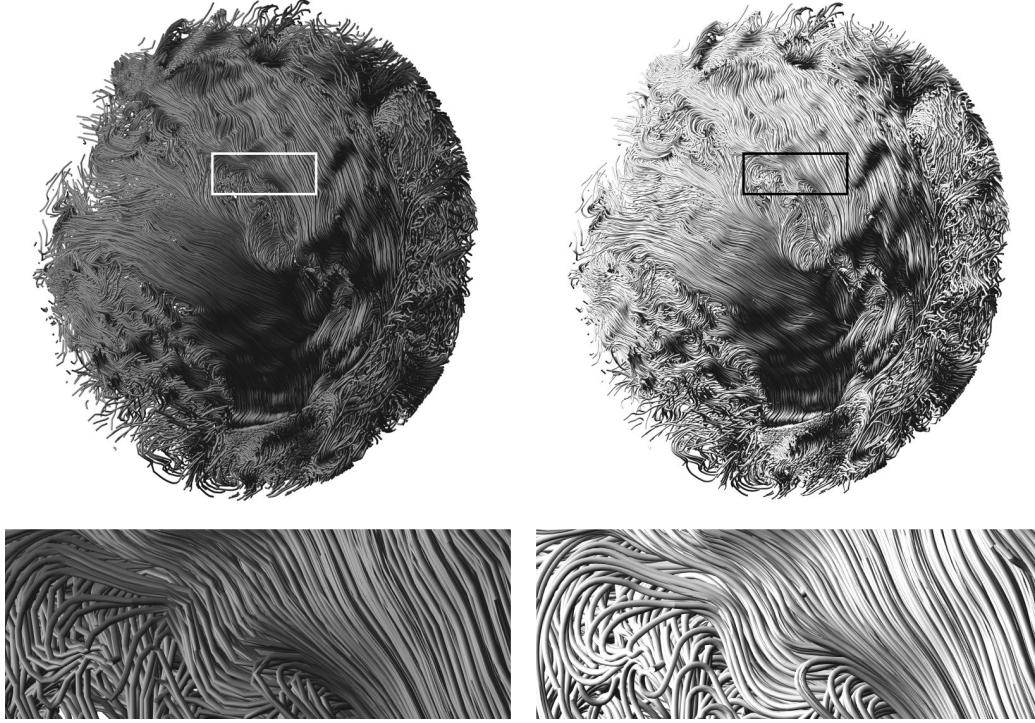
Figure 11: Our algorithm (right) applied to the result of a simulation of the magnetic field of a star (around 9000 curves) from [5].

	Dataset 9a	Dataset 9b	Dataset 9c	Dataset 10	Dataset 11
average error	0.03%	0.03%	0.03%	0.15%	0.34%
maximum error	1.3%	1.3%	3.5%	3%	3.8%
ave. comp. time	0.39	0.45	0.31	0.03	0.35
max. comp. time	1.71	1.71	0.57	1.28	13.28
total comp. time	950	690	630	160	3080

Table 2: Average and maximum relative error (compared to the typical dimension of the scene) of our curve approximation algorithm and average, maximum and total computation time in seconds, computed on the range of all the curve samples composing the 5 large datasets of Figures 9a, 9b, 9c, 10, and 11.

	Dataset 9a	Dataset 9b	Dataset 9c	Dataset 10	Dataset 11
Smoothing	$\approx 10^{-3}$	$\approx 10^{-3}$	$\approx 10^{-3}$	$\approx 2 \times 10^{-3}$	$\approx 3 \times 10^{-3}$
Spline Sampling	1.71	1.71	0.57	1.27	13.22
Points relaxation	$\approx 2 \times 10^{-4}$	$\approx 10^{-4}$	$\approx 10^{-4}$	$\approx 8 \times 10^{-3}$	0.064
Interpolation	$\approx 3 \times 10^{-4}$	$\approx 3 \times 10^{-4}$	$\approx 3 \times 10^{-4}$	0.096	0.02

Table 3: Maximum computation time in seconds for each part of the algorithm applied to each sample curve composing the 5 datasets of Figures 9a, 9b, 9c, 10, and 11.
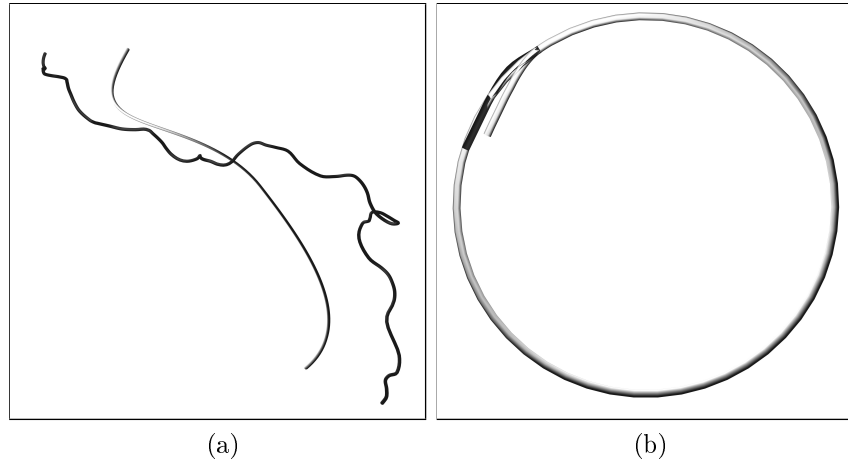

| (a) | (b) |

Figure 12: Issues resulting from a wrong choice of the number of elements. On the left, our curve approximation made of too few elements (in grey) for a very long input curve (in black). On the right, our approximation made of too many elements (in grey) for a very short input curve (in black).

As mentioned above, for those complex datasets we also had to adapt the number of helical elements used in the approximation depending on the length of the input curves. Without this adaptive scheme, two degenerate cases could make our algorithm fail. On the one hand, with too small a number of elements on a lengthy curve, the algorithm may not match the input curve accurately, as shown in Figure 12a. On the other hand, approximating a small curve with too high a number of elements may yield very close break points, which could sometimes be inverted during the relaxation process and result in the looping phenomenon depicted in Figure 12b.

Apart from these two extreme, degenerate cases, our algorithm behaves in a very *robust* way on all the data sets we have tested.

7. Conclusion

In this paper, we have presented the 3d floating tangent method, a new 3d method for robustly and efficiently approximating Bézier splines of arbitrary curved geometry with smooth piecewise helices. Our method is a generalization of our previous 2d method and builds upon a recent theorem proposed by Ghosh for interpolating 2 points and 2 tangents with a single short helix. We have proposed a complete proof of this theorem which validates the correctness of our algorithm in the general case. Finally, we have demonstrated that our new algorithm was simple, fast, accurate and highly scalable by successfully testing it on a wide range of curve data sets, either synthetically designed by an artist or resulting from image-based 3d reconstructions. We believe our method could open the way for reliably compressing large curve datasets into smooth, compact and easily manipulable primitives.

References

[1] Alt, H., Godau, M., 1995. Computing the Fréchet distance between two polygonal curves. Internat. J. Comput. Geom. Appl. 5, 75–91.

[2] Bergbom, M., Museth, K., Roble, D., 2007. Robust fitting of super-helices to parametric curves. In: ACM SIGGRAPH 2007 posters. SIGGRAPH '07. ACM, New York, NY, USA.
URL http://doi.acm.org/10.1145/1280720.1280746

[3] Bertails, F., Audoly, B., Cani, M.-P., Querleux, B., Leroy, F., Lévêque, J. L., 2006. Super-helices for predicting the dynamics of natural hair. ACM Trans. Graph. 25 (3), 1180–1187.

[4] Bolton, K., 1975. Biarc curves. Journal of Computer Aided Design 7, 89–92.

[5] Brown, B. P., Miesch, M. S., Browning, M. K., Brun, A. S., Toomre, J., 2011. Magnetic cycles in a convective dynamo simulation of a young solar-type star. The Astrophysical Journal 731 (1), 69.
URL http://stacks.iop.org/0004-637X/731/i=1/a=69

[6] Chen, X., Neubert, B., Xu, Y.-Q., Deussen, O., Kang, S. B., December 2008. Sketch-based tree modeling using markov random field. ACM Trans. Graph. 27, 109:1–109:9.
URL http://doi.acm.org/10.1145/1409060.1409062

[7] Chouaieb, N., Goriely, A., Maddocks, J. H., 2006. Helices. Proc Natl Acad Sci U S A 103 (25), 9398–403.
URL http://www.biomedsearch.com/nih/Helices/16769895.html

[8] Christopher, J. A., Swanson, R., Baldwin, T. O., 1996. Algorithms for finding the axis of a helix: Fast rotational and parametric least-squares methods. Computers Chemistry 20 (3), 339 – 345.
URL http://www.sciencedirect.com/science/article/pii/0097848595000755

[9] Derouet-Jourdan, A., Bertails-Descoubes, F., Thollot, J., 2010. Stable inverse dynamic curves. ACM Trans. Graph. 29 (6), 137.

[10] Derouet-Jourdan, A., Bertails-Descoubes, F., Thollot, J., 2011. 3d inverse dynamic modeling of strands. In: ACM SIGGRAPH 2011 Posters. SIGGRAPH '11. ACM, New York, NY, USA, pp. 55:1–55:1.
URL http://doi.acm.org/10.1145/2037715.2037778

[11] Eiter, T., Mannila, H., 1994. Computing discrete Fréchet distance. Tech. rep., Technische Universitat Wien.

[12] Enkhbayar, P., Damdinsuren, S., Osaki, M., Matsushima, N., 2008. Helfit: Helix fitting by a total least squares method. Computational Biology and Chemistry 32 (4), 307 – 310.
URL http://www.sciencedirect.com/science/article/pii/S1476927108000418

[13] Ghosh, S., December 2010. Geometric approximation of curves and singularities of secant maps. A differential geometric approach. PhD dissertation, University of Groningen, Johann Bernoulli Institute for Mathe-

matics and Computer Science, advisors: G. Vegter and J. Rieger, 185 pages.

[14] Goriely, A., Neukirch, S., Hausrath, A., 2009. Polyhelices through n points. IJBRA 5 (2), 118–132.

[15] Gould, T., Harrington, B., Hurst, N., MenTaLguY, 2003. Inkscape.
URL http://inkscape.org/

[16] Jakob, W., Moon, J. T., Marschner, S., December 2009. Capturing hair assemblies fiber by fiber. ACM Trans. Graph. 28, 164:1–164:9.
URL http://doi.acm.org/10.1145/1618452.1618510

[17] Kim, T.-Y., Neumann, U., July 2002. Interactive multiresolution hair modeling and editing. ACM Trans. Graph. 21, 620–629.
URL http://doi.acm.org/10.1145/566654.566627

[18] McCrae, J., Singh, K., 2009. Sketch-based path design. In: Proceedings of Graphics Interface 2009. GI '09. Canadian Information Processing Society, Toronto, Ont., Canada, Canada, pp. 95–102.
URL http://dl.acm.org/citation.cfm?id=1555880.1555906

[19] Nievergelt, Y., 1997. Fitting helices to data by total least squares. Computer Aided Geometric Design 14 (8), 707–718.

[20] Paris, S., Chang, W., Kozhushnyan, O. I., Jarosz, W., Matusik, W., Zwicker, M., Durand, F., August 2008. Hair photobooth: geometric and photometric acquisition of real hairstyles. ACM Trans. Graph. 27, 30:1–30:9.
URL http://doi.acm.org/10.1145/1360612.1360629

[21] Piuze, E., Kry, P. G., Siddiqi, K., 2011. Generalized helicoids for modeling hair geometry. Comput. Graph. Forum 30 (2), 247–256.

[22] Rohmer, D., Sitek, A., Gullberg, G. T., Nov 2007. Reconstruction and visualization of fiber and laminar structure in the normal human heart from ex vivo diffusion tensor magnetic resonance imaging (dtmri) data. Investigative Radiology 42 (11), 777–789.

[23] Safonova, A., Rossignac, J., 2003. Compressed piecewise-circular approximations of 3d curves. Computer-Aided Design 35 (6), 533–547.

[24] Savadjiev, P., Campbell, J. S. W., Pike, G. B., Siddiqi, K., 2006. 3d curve inference for diffusion mri regularization and fibre tractography. Medical Image Analysis 10 (5), 799–813.
URL http://www.ncbi.nlm.nih.gov/pubmed/16919994

[25] Schneider, P. J., 1990. Graphics gems. Academic Press Professional, Inc., San Diego, CA, USA, Ch. An algorithm for automatically fitting digitized curves, pp. 612–626.

[26] Sloss, J. M., 1970. The bending of space curves into piecewise helical curves. Pacific Journal of Mathematics. 32, 231–239.

[27] Tan, P., Zeng, G., Wang, J., Kang, S. B., Quan, L., July 2007. Image-based tree modeling. ACM Trans. Graph. 26, 87:1–87:7.
URL http://doi.acm.org/10.1145/1276377.1276486

[28] Wang, L., Yu, Y., Zhou, K., Guo, B., Jul. 2009. Example-based hair geometry synthesis. ACM Trans. Graph. 28, 56:1–56:9.
URL http://doi.acm.org/10.1145/1531326.1531362

Appendix A. Full proof of Ghosh's theorem

In this appendix, we give the complete proof of Ghosh's theorem:

Theorem 5.1. *Given two points $\boldsymbol{p}_0$ and $\boldsymbol{p}_1$ such that $\boldsymbol{p}_0 \neq \boldsymbol{p}_1$ and two tangents $\boldsymbol{t}_0$ and $\boldsymbol{t}_1$ such that $\boldsymbol{t}_1 \neq \pm \boldsymbol{t}_0$, there exists a unique short helix starting at $\boldsymbol{p}_0$ with tangent $\boldsymbol{t}_0$ and ending at $\boldsymbol{p}_1$ with tangent $\boldsymbol{t}_1$ if and only if*

$$\langle \boldsymbol{p}_1 - \boldsymbol{p}_0 \, , \, \boldsymbol{t}_1 - \boldsymbol{t}_0 \rangle = 0. \tag{A.1}$$

Appendix A.1. Preliminaries

Before entering the core of the proof of Theorem 5.1, we introduce the Frenet Frame and the Darboux vector for a general curve. We then introduce another moving frame based on the normal from the Frenet frame and the Darboux vector. We use this adapted frame to describe a helix and its tangent and to prove Theorem 5.1.

Appendix A.1.1. Frenet Frame and Darboux vector

We proceed as Ghosh does, but with a different convention for the Frenet frame. Let $\boldsymbol{\alpha} : I \to \mathbb{R}^3$ be a 3d curve parametrized by its arc-length. Let $\{\mathbf{t}, \mathbf{n}, \mathbf{b}\}$ be its Frenet frame, which satisfies

$$\begin{pmatrix} \mathbf{t}' \\ \mathbf{n}' \\ \mathbf{b}' \end{pmatrix} = \begin{pmatrix} 0 & \kappa & 0 \\ -\kappa & 0 & \tau \\ 0 & -\tau & 0 \end{pmatrix} \begin{pmatrix} \mathbf{t} \\ \mathbf{n} \\ \mathbf{b} \end{pmatrix} \tag{A.2}$$

with $\kappa(s)$ the curvature and $\tau(s)$ the torsion along the curve $\boldsymbol{\alpha}$. Let us write then

$$\boldsymbol{\Omega} = \tau \mathbf{t} + \kappa \mathbf{b} \tag{A.3}$$

the Darboux vector, which satisfies

$$\mathbf{t}' = \boldsymbol{\Omega} \times \mathbf{t} \qquad \mathbf{n}' = \boldsymbol{\Omega} \times \mathbf{n} \qquad \mathbf{b}' = \boldsymbol{\Omega} \times \mathbf{b}. \tag{A.4}$$

We define $\omega = \sqrt{\kappa^2 + \tau^2}$ the norm of $\boldsymbol{\Omega}$ and $\bar{\boldsymbol{\Omega}}$ the normal vector $\frac{1}{\omega}\boldsymbol{\Omega} = \bar{\tau}\mathbf{t} + \bar{\kappa}\mathbf{b}$. Since $\bar{\boldsymbol{\Omega}}$ is orthogonal to the normal vector $\mathbf{n}$, we introduce the frame $\{\mathbf{n}, \mathbf{w}, \bar{\boldsymbol{\Omega}}\}$ with

$$\mathbf{w} = \bar{\boldsymbol{\Omega}} \times \mathbf{n} = -\bar{\kappa}\mathbf{t} + \bar{\tau}\mathbf{b}.$$

34

Then, we have

$$\mathbf{t} = \bar{\tau}\bar{\boldsymbol{\Omega}} - \bar{\kappa}\mathbf{w} \text{ and } \mathbf{b} = \bar{\kappa}\bar{\boldsymbol{\Omega}} + \bar{\tau}\mathbf{w}. \tag{A.5}$$

Since $\bar{\boldsymbol{\Omega}} \times \mathbf{n} = \mathbf{w}$ and $\bar{\boldsymbol{\Omega}}$ is orthogonal to $\mathbf{n}$ the moving frame $\{\mathbf{n}, \mathbf{w}, \bar{\boldsymbol{\Omega}}\}$ is orthonormal. Moreover, we have

$$\begin{aligned}
\mathbf{n}' &= -\kappa\mathbf{t} + \tau\mathbf{b} \\
&= \omega\mathbf{w} \\
\bar{\boldsymbol{\Omega}}' &= \bar{\tau}\mathbf{t}' + \bar{\kappa}\mathbf{b}' + \bar{\tau}'\mathbf{t} + \bar{\kappa}'\mathbf{b} \\
&= \bar{\tau}\kappa\mathbf{n} - \bar{\kappa}\tau\mathbf{n} + \bar{\tau}'(\bar{\tau}\bar{\boldsymbol{\Omega}} - \bar{\kappa}\mathbf{w}) + \bar{\kappa}'(\bar{\kappa}\bar{\boldsymbol{\Omega}} + \bar{\tau}\mathbf{w}) \\
&= (\bar{\tau}\kappa - \bar{\kappa}\tau)\mathbf{n} + (\bar{\tau}'\bar{\tau} + \bar{\kappa}'\bar{\kappa})\bar{\boldsymbol{\Omega}} + (\bar{\kappa}'\bar{\tau} - \bar{\tau}'\bar{\kappa})\mathbf{w}.
\end{aligned}$$

Now, the following equalities

$$\bar{\tau}\kappa - \bar{\kappa}\tau = \frac{\tau\kappa}{\omega} - \frac{\kappa\tau}{\omega} = 0 \text{ and } \bar{\tau}'\bar{\tau} + \bar{\kappa}'\bar{\kappa} = \frac{1}{2}(\bar{\tau}^2 + \bar{\kappa}^2)' = 0,$$

give a simplification of $\bar{\boldsymbol{\Omega}}'$ and we have

$$\begin{aligned}
\bar{\boldsymbol{\Omega}}' &= (\bar{\kappa}'\bar{\tau} - \bar{\tau}'\bar{\kappa})\mathbf{w} \\
&= \gamma\mathbf{w}
\end{aligned}$$

with $\gamma = \bar{\kappa}'\bar{\tau} - \bar{\tau}'\bar{\kappa}$. We get

$$\begin{aligned}
\mathbf{w}' &= \bar{\boldsymbol{\Omega}}' \times \mathbf{n} + \bar{\boldsymbol{\Omega}} \times \mathbf{n}' \\
&= \gamma(\mathbf{w} \times \mathbf{n}) + \omega(\bar{\boldsymbol{\Omega}} \times \mathbf{w}) \\
&= -\gamma\bar{\boldsymbol{\Omega}} - \omega\mathbf{n},
\end{aligned}$$

and finally, the frame $\{\mathbf{n}, \mathbf{w}, \bar{\boldsymbol{\Omega}}\}$ satisfies

$$\begin{pmatrix} \mathbf{n}' \\ \mathbf{w}' \\ \bar{\boldsymbol{\Omega}}' \end{pmatrix} = \begin{pmatrix} 0 & \omega & 0 \\ -\omega & 0 & -\gamma \\ 0 & \gamma & 0 \end{pmatrix} \begin{pmatrix} \mathbf{n} \\ \mathbf{w} \\ \bar{\boldsymbol{\Omega}} \end{pmatrix}. \tag{A.6}$$

Appendix A.1.2. Equation of a helix

Now, we follow the next step of Ghosh's proof, by describing a helix and its tangent in the adapted frame $\{\mathbf{n}, \mathbf{w}, \bar{\boldsymbol{\Omega}}\}$.

For a helix, the curvature and the torsion are constant. Thus, $\bar{\kappa}$, $\bar{\tau}$ and ω

35

are constant. In this case, the Darboux vector $\mathbf{\Omega}$ and the vector $\bar{\mathbf{\Omega}}$ are also constant which is satisfied by $\gamma = 0$ which means, from Equation (A.6), that $\bar{\mathbf{\Omega}}'$ is the zero vector and thus that $\bar{\mathbf{\Omega}}$ is constant.

In order to write the equation of a helix, we use the function φ defined with

$$\varphi(s) = \int_0^s \omega \, \mathrm{d}u = \omega s$$

and the functions C and S given by

$$C(s) = \int_0^s \cos \varphi(u) \, \mathrm{d}u = \frac{\sin \omega s}{\omega} = \frac{\sin \varphi}{\omega}$$
$$S(s) = \int_0^s \sin \varphi(u) \, \mathrm{d}u = \frac{1 - \cos \omega s}{\omega} = \frac{1 - \cos \varphi}{\omega}.$$

Let us write $\boldsymbol{\alpha}$ the equation of a helix parametrized by its arc-length and starting at point $\mathbf{p}_0$ with the Frenet frame $\{\mathbf{t}_0, \mathbf{n}_0, \mathbf{b}_0\}$ from which we have the frame $\{\mathbf{n}_0, \mathbf{w}_0, \bar{\mathbf{\Omega}} = \bar{\mathbf{\Omega}}_0\}$ as we defined in Subsection Appendix A.1.1. At the point at abscissa s, we have

$$\boldsymbol{\alpha}'(s) = \mathbf{t}(s) = \bar{\tau}\bar{\mathbf{\Omega}} - \bar{\kappa}\mathbf{w}.$$

Now, from the differential equation (A.6), since for a helix $\gamma = 0$, we have

$$\begin{cases} \mathbf{w}' & = & -\omega\mathbf{n} \\ \mathbf{n}' & = & \omega\mathbf{w} \end{cases}$$

that has the solution

$$\begin{cases} \mathbf{w} & = & \cos \omega s \mathbf{w}_0 - \sin \omega s \mathbf{n}_0 \\ \mathbf{n} & = & \sin \omega s \mathbf{w}_0 + \cos \omega s \mathbf{n}_0. \end{cases}$$

Thus, we write

$$\boldsymbol{\alpha}'(s) = \mathbf{t}(s) = \bar{\tau}\bar{\mathbf{\Omega}} - \bar{\kappa}(\cos \omega s \mathbf{w}_0 - \sin \omega s \mathbf{n}_0) \tag{A.7}$$

and by integrating (A.7),

$$\boldsymbol{\alpha}(s) = \mathbf{p}_0 + \bar{\tau}s\bar{\mathbf{\Omega}} - \bar{\kappa}(C(s)\mathbf{w}_0 - S(s)\mathbf{n}_0), \tag{A.8}$$

which are the equations of $\boldsymbol{\alpha}$ and T respectively in the frame $\{\mathbf{n}_0, \mathbf{w}_0, \bar{\mathbf{\Omega}}\}$.

Now, we write those equations in the constant orthogonal frame $\{\bar{\boldsymbol{\Omega}}, \mathbf{t}_0 - \bar{\tau}\bar{\boldsymbol{\Omega}}, \mathbf{t}_0 \times \bar{\boldsymbol{\Omega}}\}$ introduced by Ghosh. From (A.2), (A.4) and (A.5), we have

$$\bar{\kappa}\mathbf{w}_0 = \bar{\tau}\bar{\boldsymbol{\Omega}} - \mathbf{t}_0 \quad \text{and} \quad \bar{\kappa}\mathbf{n}_0 = -\mathbf{t}_0 \times \bar{\boldsymbol{\Omega}}$$

it follows that

$$\boldsymbol{\alpha}(s) = \mathbf{p}_0 + \bar{\tau}s\bar{\boldsymbol{\Omega}} + C(s)(\mathbf{t}_0 - \bar{\tau}\bar{\boldsymbol{\Omega}}) - S(s)(\mathbf{t}_0 \times \bar{\boldsymbol{\Omega}}) \tag{A.9}$$

$$\mathbf{t}(s) = \mathbf{t}_0 + (\cos \omega s - 1)(\mathbf{t}_0 - \bar{\tau}\bar{\boldsymbol{\Omega}}) - \sin \omega s(\mathbf{t}_0 \times \bar{\boldsymbol{\Omega}}), \tag{A.10}$$

which can be rewritten as

$$\boldsymbol{\alpha}(\varphi) = \mathbf{p}_0 + \bar{\tau}\frac{\varphi}{\omega}\bar{\boldsymbol{\Omega}} + \frac{\sin \varphi}{\omega}(\mathbf{t}_0 - \bar{\tau}\bar{\boldsymbol{\Omega}})$$
$$- \frac{1 - \cos \varphi}{\omega}(\mathbf{t}_0 \times \bar{\boldsymbol{\Omega}}) \tag{A.11}$$

$$\mathbf{t}(\varphi) = \mathbf{t}_0 + (\cos \varphi - 1)(\mathbf{t}_0 - \bar{\tau}\bar{\boldsymbol{\Omega}}) - \sin \varphi(\mathbf{t}_0 \times \bar{\boldsymbol{\Omega}}), \tag{A.12}$$

with the change of variable $\varphi = \omega s$. We can also conclude that the vector $\bar{\boldsymbol{\Omega}}$ is the unit axis of the helix.

We now define a *short helix* similarly as in [13]:

Definition. *A helix of axis $\bar{\boldsymbol{\Omega}}$ is called a short helix when its projection onto the plane orthogonal to $\bar{\boldsymbol{\Omega}}$ is a circle arc that is not a full circle.*

Considering Equation (A.9), the projection of the helix onto the plane orthogonal to $\bar{\boldsymbol{\Omega}}$ reads

$$\boldsymbol{\alpha}_\perp(\varphi) = \mathbf{p}_0 + \frac{\sin \varphi}{\omega}(\mathbf{t}_0 - \bar{\tau}\bar{\boldsymbol{\Omega}}) - \frac{1 - \cos \varphi}{\omega}(\mathbf{t}_0 \times \bar{\boldsymbol{\Omega}})$$

which is the equation of a circle. This curve is a short circle arc if we have

$$\varphi \in [0, \varphi_*] \text{ and } \varphi_* \in [0, 2\pi[.$$

Appendix A.2. Proof of the theorem

Now, we prove Theorem 5.1. Proving that the condition (A.1) is necessary is straightforward with Equations (A.7) and (A.8). Indeed, if we consider two points $\mathbf{p}_0$ and $\mathbf{p}_1$ and two tangents $\mathbf{t}_0$ and $\mathbf{t}_1$, and if we assume the existence of a helix of equation $\boldsymbol{\alpha}$ with the tangent $\mathbf{t}$ that interpolates the two points

37

and the two tangents, we have

$$\mathbf{p}_1 - \mathbf{p}_0 = \boldsymbol{\alpha}(l) - \boldsymbol{\alpha}(0) = \bar{\tau}\bar{\boldsymbol{\Omega}} - \bar{\kappa}(C(l)\mathbf{w}_0 - S(l)\mathbf{n}_0)$$
$$\mathbf{t}_1 - \mathbf{t}_0 = \mathbf{t}(l) - \mathbf{t}_0 = -\bar{\kappa}((\cos\omega l - 1)\mathbf{w}_0 - \sin\omega l\mathbf{n}_0),$$

provided that $\boldsymbol{\alpha}(l) = \mathbf{p}_1$ and $\mathbf{t}(l) = \mathbf{t}_1$. Then, we get

$$\langle \mathbf{p}_1 - \mathbf{p}_0 \,, \, \mathbf{t}_1 - \mathbf{t}_0 \rangle = \bar{\kappa}^2(C(l)(\cos\omega l - 1) - S(l)\sin\omega l)$$
$$= 0.$$

Proving that Condition (A.1) is sufficient requires more calculations.

First, we need an intermediate lemma which gives a first characterization of the parameters of the helix. Then, we use this characterization to prove the existence and uniqueness of the helix.

For the rest of the proof, we consider two points $\mathbf{p}_0$ and $\mathbf{p}_1$ and two unit vectors $\mathbf{t}_0$ and $\mathbf{t}_1$ satisfying Condition (A.1). Following Ghosh's proof, let us define

$$t_0 = \langle \mathbf{t}_0 \,, \, \mathbf{t}_1 \rangle$$

and let us assume that $\mathbf{t}_1 \neq \pm\mathbf{t}_0$ and so

$$t_0 \in \,]{-1} \,; 1[\,.$$

Lemma 5.2. *The helix of parameters ω, $\bar{\tau}$, φ_* and $\bar{\boldsymbol{\Omega}}$ interpolates the points $\boldsymbol{p}_0$ and $\boldsymbol{p}_1$ with respective tangents $\boldsymbol{t}_0$ and $\boldsymbol{t}_1$ if and only if*

$$\begin{cases} \omega|\langle \boldsymbol{p}_1 - \boldsymbol{p}_0 \,, \, \boldsymbol{t}_1 \times \boldsymbol{t}_0 \rangle| = \\ \qquad -\dfrac{\sqrt{2}(1-t_0)(\varphi_* \cos\frac{\varphi_*}{2} - 2\sin\frac{\varphi_*}{2})}{1 - \cos\varphi_*}\sqrt{t_0 - \cos\varphi_*} \\ \omega\langle \boldsymbol{p}_1 - \boldsymbol{p}_0 \,, \, \boldsymbol{t}_1 + \boldsymbol{t}_0 \rangle = \\ \qquad \dfrac{2}{1 - \cos\varphi_*}[(1 - t_0)\sin\varphi_* + \varphi_*(t_0 - \cos\varphi_*)] \\ \bar{\tau} = \mathrm{sign}\langle \boldsymbol{p}_1 - \boldsymbol{p}_0 \,, \, \boldsymbol{t}_1 \times \boldsymbol{t}_0 \rangle\sqrt{\frac{t_0 - \cos\varphi_*}{1 - \cos\varphi_*}} \\ \bar{\boldsymbol{\Omega}} = \frac{1}{1+t_0}\left(\bar{\tau}(\boldsymbol{t}_1 + \boldsymbol{t}_0) + \left(\cot\frac{\varphi_*}{2}\right)(\boldsymbol{t}_1 \times \boldsymbol{t}_0)\right). \end{cases} \qquad (A.13)$$

Let us introduce the following quantities,

$$N(\varphi) = (1 - t_0)\sin\varphi + \varphi(t_0 - \cos\varphi) \tag{A.14}$$

$$D(\varphi) = (\varphi\cos\frac{\varphi}{2} - 2\sin\frac{\varphi}{2})\sqrt{t_0 - \cos\varphi}. \tag{A.15}$$

Condition (A.13) becomes

$$
\begin{cases}
\omega|\langle \mathbf{p}_1 - \mathbf{p}_0 \,,\, \mathbf{t}_1 \times \mathbf{t}_0\rangle| = -\frac{\sqrt{2}(1-t_0)}{1-\cos\varphi_*}D(\varphi_*) \\
\omega\langle \mathbf{p}_1 - \mathbf{p}_0 \,,\, \mathbf{t}_1 + \mathbf{t}_0\rangle = \frac{2}{1-\cos\varphi_*}N(\varphi_*) \\
\bar{\tau} = \mathrm{sign}\langle \mathbf{p}_1 - \mathbf{p}_0 \,,\, \mathbf{t}_1 \times \mathbf{t}_0\rangle\sqrt{\frac{t_0-\cos\varphi_*}{1-\cos\varphi_*}} \\
\bar{\boldsymbol{\Omega}} = \frac{1}{1+t_0}\left(\bar{\tau}(\mathbf{t}_1 + \mathbf{t}_0) + \left(\cot\frac{\varphi_*}{2}\right)(\mathbf{t}_1 \times \mathbf{t}_0)\right).
\end{cases}
\tag{A.16}
$$

Appendix A.2.1. Proof of the lemma.

To prove Lemma 5.2, we follow the steps of Ghosh's proof, and particularly the key idea of the whole proof, which is cleverly to write the equations of the helix and its tangent in a well-chosen basis of $\mathbb{R}^3$. The main difference with Ghosh's proof here is that we fully characterize the parameter φ_*.

Let us assume the existence of a short helix $\mathscr{H}$ parametrized by arclength which interpolates the points $\mathbf{p}_0$ and $\mathbf{p}_1$ with $\mathbf{t}_0$ and $\mathbf{t}_1$ as respective tangents. We denote $\boldsymbol{\alpha}$ the equation of this helix and $\mathbf{t}$ the equation of its tangent.

We have then

$$\boldsymbol{\alpha}(\varphi_*) = \mathbf{p}_1 = \mathbf{p}_0 + \bar{\tau}\frac{\varphi_*}{\omega}\bar{\boldsymbol{\Omega}} + \frac{\sin\varphi_*}{\omega}(\mathbf{t}_0 - \bar{\tau}\bar{\boldsymbol{\Omega}}) \tag{A.17}$$

$$- \frac{1 - \cos\varphi_*}{\omega}(\mathbf{t}_0 \times \bar{\boldsymbol{\Omega}}) \tag{A.18}$$

$$\mathbf{t}(\varphi_*) = \mathbf{t}_1 = \mathbf{t}_0 + (\cos\varphi_* - 1)(\mathbf{t}_0 - \bar{\tau}\bar{\boldsymbol{\Omega}}) - \sin\varphi_*(\mathbf{t}_0 \times \bar{\boldsymbol{\Omega}}), \tag{A.19}$$

which can be written as

$$
\mathbf{p}_1 - \mathbf{p}_0 = \frac{1}{\omega}(\bar{\tau}\varphi_*\bar{\boldsymbol{\Omega}} + \sin\varphi_*(\mathbf{t}_0 - \bar{\tau}\bar{\boldsymbol{\Omega}}) \\
- (1 - \cos\varphi_*)(\mathbf{t}_0 \times \bar{\boldsymbol{\Omega}}))
\tag{A.20}
$$

$$\mathbf{t}_1 - \mathbf{t}_0 = (\cos\varphi_* - 1)(\mathbf{t}_0 - \bar{\tau}\bar{\boldsymbol{\Omega}}) - \sin\varphi_*(\mathbf{t}_0 \times \bar{\boldsymbol{\Omega}}). \tag{A.21}$$

If we define

$$\gamma(\varphi) = \boldsymbol{\alpha}(\varphi) - \mathbf{p}_0 \tag{A.22}$$

$$\theta(\varphi) = \mathbf{t}(\varphi) - \mathbf{t}_0, \tag{A.23}$$

we have

$$\begin{cases} \mathbf{p}_1 - \mathbf{p}_0 & = \gamma(\varphi_*) \\ \mathbf{t}_1 - \mathbf{t}_0 & = \theta(\varphi_*). \end{cases} \tag{A.24}$$

Helix $\mathscr{H}$ exists if and only if the conjunction of those two equalities holds. Let $(\mathbf{e}_1, \mathbf{e}_2, \mathbf{e}_3)$ be the basis of $\mathbb{R}^3$, introduced by Ghosh such that:

$$\mathbf{e}_1 = \frac{1}{\sqrt{2(1 + t_0)}}(\mathbf{t}_1 + \mathbf{t}_0),$$

$$\mathbf{e}_2 = \frac{1}{\sqrt{1 - t_0^2}}(\mathbf{t}_1 \times \mathbf{t}_0),$$

$$\mathbf{e}_3 = \frac{1}{\sqrt{2(1 - t_0)}}(\mathbf{t}_1 - \mathbf{t}_0).$$

Ghosh proved that this basis is orthonormal, with $\mathbf{e}_1 \times \mathbf{e}_2 = \mathbf{e}_3$. If we write Equation (A.24) in the basis $\{\mathbf{e}_1, \mathbf{e}_2, \mathbf{e}_3\}$, we obtain, since the basis $\{\mathbf{e}_1, \mathbf{e}_2, \mathbf{e}_3\}$ is orthonormal

$$\langle \mathbf{p}_1 - \mathbf{p}_0 , \mathbf{e}_1 \rangle \mathbf{e}_1 + \langle \mathbf{p}_1 - \mathbf{p}_0 , \mathbf{e}_2 \rangle \mathbf{e}_2 + \langle \mathbf{p}_1 - \mathbf{p}_0 , \mathbf{e}_3 \rangle \mathbf{e}_3$$
$$= \langle \gamma(\varphi_*) , \mathbf{e}_1 \rangle \mathbf{e}_1 + \langle \gamma(\varphi_*) , \mathbf{e}_2 \rangle \mathbf{e}_2 + \langle \gamma(\varphi_*) , \mathbf{e}_3 \rangle \mathbf{e}_3$$
$$\langle \mathbf{t}_1 - \mathbf{t}_0 , \mathbf{e}_1 \rangle \mathbf{e}_1 + \langle \mathbf{t}_1 - \mathbf{t}_0 , \mathbf{e}_2 \rangle \mathbf{e}_2 + \langle \mathbf{t}_1 - \mathbf{t}_0 , \mathbf{e}_3 \rangle \mathbf{e}_3$$
$$= \langle \theta(\varphi_*) , \mathbf{e}_1 \rangle \mathbf{e}_1 + \langle \theta(\varphi_*) , \mathbf{e}_2 \rangle \mathbf{e}_2 + \langle \theta(\varphi_*) , \mathbf{e}_3 \rangle \mathbf{e}_3$$

which is equivalent to

$$\langle \mathbf{p}_1 - \mathbf{p}_0 , \mathbf{t}_1 + \mathbf{t}_0 \rangle = \langle \gamma(\varphi_*) , \mathbf{t}_1 + \mathbf{t}_0 \rangle \tag{A.25}$$

$$\langle \mathbf{p}_1 - \mathbf{p}_0 , \mathbf{t}_1 \times \mathbf{t}_0 \rangle = \langle \gamma(\varphi_*) , \mathbf{t}_1 \times \mathbf{t}_0 \rangle \tag{A.26}$$

$$\langle \mathbf{p}_1 - \mathbf{p}_0 , \mathbf{t}_1 - \mathbf{t}_0 \rangle = \langle \gamma(\varphi_*) , \mathbf{t}_1 - \mathbf{t}_0 \rangle \tag{A.27}$$

$$\langle \mathbf{t}_1 - \mathbf{t}_0 , \mathbf{t}_1 + \mathbf{t}_0 \rangle = \langle \theta(\varphi_*) , \mathbf{t}_1 + \mathbf{t}_0 \rangle \tag{A.28}$$

$$\langle \mathbf{t}_1 - \mathbf{t}_0 , \mathbf{t}_1 \times \mathbf{t}_0 \rangle = \langle \theta(\varphi_*) , \mathbf{t}_1 \times \mathbf{t}_0 \rangle \tag{A.29}$$

$$\langle \mathbf{t}_1 - \mathbf{t}_0 , \mathbf{t}_1 - \mathbf{t}_0 \rangle = \langle \theta(\varphi_*) , \mathbf{t}_1 - \mathbf{t}_0 \rangle. \tag{A.30}$$

Now, we are going to evaluate those six equations to deduce a conjunction of properties of $\gamma(s)$ and $\theta(s)$ equivalent to the existence of the helix. We start by calculating some inner products.

First, we have
$$\langle \mathbf{t}_0 \,, \bar{\boldsymbol{\Omega}} \rangle = \langle \mathbf{t}_1 \,, \bar{\boldsymbol{\Omega}} \rangle = \bar{\tau}$$

This result is trivial by Equation (A.19). Then, we have immediately

$$\langle \bar{\boldsymbol{\Omega}} \,, \mathbf{t}_1 + \mathbf{t}_0 \rangle = 2\bar{\tau} \tag{A.31}$$
$$\langle \bar{\boldsymbol{\Omega}} \,, \mathbf{t}_1 - \mathbf{t}_0 \rangle = 0 \tag{A.32}$$
$$\langle \mathbf{t}_0 - \bar{\tau}\bar{\boldsymbol{\Omega}} \,, \mathbf{t}_1 + \mathbf{t}_0 \rangle = 1 + t_0 - 2\bar{\tau}^2 \tag{A.33}$$
$$\langle \mathbf{t}_0 - \bar{\tau}\bar{\boldsymbol{\Omega}} \,, \mathbf{t}_1 - \mathbf{t}_0 \rangle = t_0 - 1. \tag{A.34}$$

We now have to calculate those inner products:

$$\langle \mathbf{t}_0 \times \bar{\boldsymbol{\Omega}} \,, \mathbf{t}_1 \times \mathbf{t}_0 \rangle$$
$$\langle \mathbf{t}_0 \times \bar{\boldsymbol{\Omega}} \,, \mathbf{t}_1 + \mathbf{t}_0 \rangle$$
$$\langle \mathbf{t}_0 \times \bar{\boldsymbol{\Omega}} \,, \mathbf{t}_1 - \mathbf{t}_0 \rangle.$$

Since $\mathbf{t}_0 \times \bar{\boldsymbol{\Omega}}$ is orthogonal to $\mathbf{t}_0$, the last two products are equal. To determine their value, we write, with the conjunction of (A.28), (A.29) and (A.30)

$$\langle \theta(\varphi_*) \,, \mathbf{t}_1 - \mathbf{t}_0 \rangle = ||\mathbf{t}_1 - \mathbf{t}_0||^2 = 2 - 2t_0,$$

which is equivalent to

$$2(1 - t_0) = (\cos\varphi_* - 1)(t_0 - 1) - \sin\varphi_* \langle \mathbf{t}_0 \times \bar{\boldsymbol{\Omega}} \,, \mathbf{t}_1 \rangle.$$

We deduce

$$\langle \mathbf{t}_0 \times \bar{\boldsymbol{\Omega}} \,, \mathbf{t}_1 \rangle = -(1 - t_0)\frac{1 + \cos\varphi_*}{\sin\varphi_*} = -(1 - t_0)\cot\frac{\varphi_*}{2}. \tag{A.35}$$

Finally, we have

$$\begin{aligned}
\langle \mathbf{t}_0 \times \bar{\boldsymbol{\Omega}} \,, \mathbf{t}_1 \times \mathbf{t}_0 \rangle &= \langle \mathbf{t}_1 \,, \mathbf{t}_0 \times (\mathbf{t}_0 \times \bar{\boldsymbol{\Omega}}) \rangle \\
&= \langle \mathbf{t}_1 \,, \langle \mathbf{t}_0 \,, \bar{\boldsymbol{\Omega}} \rangle \mathbf{t}_0 - \langle \mathbf{t}_0 \,, \mathbf{t}_0 \rangle \bar{\boldsymbol{\Omega}} \rangle \\
&= -\bar{\tau}(1 - t_0), \tag{A.36}
\end{aligned}$$

and we add a last result that will be useful later in the proof:

$$\langle \bar{\boldsymbol{\Omega}}\, ,\, \mathbf{t}_1 \times \mathbf{t}_0 \rangle = \langle \mathbf{t}_1\, ,\, \mathbf{t}_0 \times \bar{\boldsymbol{\Omega}} \rangle. \tag{A.37}$$

Now, we have everything we need to calculate the inner products (A.25) to (A.30). So, with (A.22), (A.31) and (A.33) we get

$$\langle \gamma(\varphi_*)\, ,\, \mathbf{t}_1 + \mathbf{t}_0 \rangle = \frac{1}{\omega} \left[2\bar{\tau}^2(\varphi_* - \sin \varphi_*) + (1 + t_0) \sin \varphi_* \right.$$
$$\left. - (1 - \cos \varphi_*) \left(-(1 - t_0) \frac{1 + \cos \varphi_*}{\sin \varphi_*} \right) \right],$$

which can be simplified to become

$$\langle \gamma(\varphi_*)\, ,\, \mathbf{t}_1 + \mathbf{t}_0 \rangle = \frac{2}{\omega} \left[\bar{\tau}^2(\varphi_* - \sin \varphi_*) + \sin \varphi_* \right].$$

Also, with (A.22), (A.35), (A.36) and (A.37), we have

$$\langle \gamma(\varphi_*)\, ,\, \mathbf{t}_1 \times \mathbf{t}_0 \rangle = \frac{1}{\omega} \left[\bar{\tau}(\varphi_* - \sin \varphi_*) + \left(-(1 - t_0) \frac{1 + \cos \varphi_*}{\sin \varphi_*} \right) \right.$$
$$\left. + \bar{\tau}\,(1 - \cos \varphi_*)(1 - t_0) \right],$$

which we simplify as

$$\langle \gamma(\varphi_*)\, ,\, \mathbf{t}_1 \times \mathbf{t}_0 \rangle = \frac{1}{\omega} \left[-\bar{\tau}(1 - t_0)(\varphi_* \cot \frac{\varphi_*}{2} - 2) \right]. \tag{A.38}$$

With a combination of (A.23), (A.31) and (A.33), we obtain

$$\langle \theta(\varphi_*)\, ,\, \mathbf{t}_1 + \mathbf{t}_0 \rangle = 2\bar{\tau}^2(1 - \cos \varphi_*) - 2(t_0 - \cos \varphi_*).$$

Since we have

$$\langle \theta(\varphi_*)\, ,\, \mathbf{t}_1 + \mathbf{t}_0 \rangle = \langle \mathbf{t}_1 - \mathbf{t}_0\, ,\, \mathbf{t}_1 + \mathbf{t}_0 \rangle$$
$$= 1 + t_0 - t_0 - 1$$
$$= 0$$

we deduce

$$\bar{\tau}^2 = \frac{t_0 - \cos \varphi_*}{1 - \cos \varphi_*}. \tag{A.39}$$

Equation (A.39) gives two important pieces of information. First, we now know that the value of φ_* is necessarily in the interval

$$I_0 = [\arccos t_0, 2\pi - \arccos t_0].$$

We also now know the square value of the torsion of our helix. We find the sign of $\bar\tau$ by examining (A.38), and using the following result that will be proven in Subsection Appendix A.2.3.

$$\forall \varphi_* \in I_0, \ \varphi_* \cot \frac{\varphi_*}{2} - 2 < 0,$$

we conclude

$$\operatorname{sign} \bar\tau = \operatorname{sign}\langle \mathbf{p}_1 - \mathbf{p}_0 \,,\, \mathbf{t}_1 \times \mathbf{t}_0 \rangle.$$

Finally, we write $\bar{\boldsymbol\Omega}$ in $\{\mathbf{e}_1, \mathbf{e}_2, \mathbf{e}_3\}$. We have

$$\bar{\boldsymbol\Omega} = \langle \bar{\boldsymbol\Omega} \,,\, \mathbf{e}_1 \rangle \mathbf{e}_1 + \langle \bar{\boldsymbol\Omega} \,,\, \mathbf{e}_2 \rangle \mathbf{e}_2 + \langle \bar{\boldsymbol\Omega} \,,\, \mathbf{e}_3 \rangle \mathbf{e}_3$$

and with a simple calculation

$$\langle \bar{\boldsymbol\Omega} \,,\, \mathbf{e}_1 \rangle = \frac{2\bar\tau}{\sqrt{2(1 + t_0)}}$$

$$\langle \bar{\boldsymbol\Omega} \,,\, \mathbf{e}_2 \rangle = -\frac{(1 - t_0) \cot \frac{\varphi_*}{2}}{\sqrt{(1 - t_0^2)}}$$

$$\langle \bar{\boldsymbol\Omega} \,,\, \mathbf{e}_3 \rangle = 0,$$

we write

$$\bar{\boldsymbol\Omega} = \frac{1}{1 + t_0} \left(\bar\tau(\mathbf{t}_1 + \mathbf{t}_0) + \left(\cot \frac{\varphi_*}{2} \right) (\mathbf{t}_1 \times \mathbf{t}_0) \right).$$

This concludes the proof of the lemma. This lemma is relevant since it provides an equivalence that we shall exploit in the theorem proof Appendix A.2.2 to prove that a helix $\mathscr{H}$ with parameters ω, $\bar\tau$, φ_* and $\bar{\boldsymbol\Omega}$ indeed interpolates the two points and two tangents when its parameters satisfy Equation (A.16). Moreover, once φ_* and ω are assumed to be unique, this lemma gives a characterization of parameters $\bar\tau$ and $\bar{\boldsymbol\Omega}$. The lemma is however not sufficient for proving the uniqueness of φ_* and ω, and we now explain how to achieve this.

Appendix A.2.2. Proof of the theorem
    We proceed with an analysis-synthesis reasoning.

- **Analysis:** We assume that such a helix exists and we precisely characterize its parameters $\bar{\boldsymbol{\Omega}}$, ω, $\bar{\tau}$ and φ_* so that we can conclude that this helix is unique. This first part was addressed by Ghosh, with a partial characterization of the parameter φ_*.

- **Synthesis:** We consider the helix with the parameters we found in the analysis to prove that it interpolates the two points and the two tangents, proving the existence of the helix. This second part was not addressed in Ghosh's proof.

Analysis. If the helix of parameters ω, $\bar{\tau}$, φ_* and $\bar{\boldsymbol{\Omega}}$ interpolates the points $\mathbf{p}_0$ and $\mathbf{p}_1$ with the respective tangents $\mathbf{t}_0$ and $\mathbf{t}_1$, then it satisfies (A.16) of Lemma 5.2. Moreover, we have

$$\langle \mathbf{p}_1 - \mathbf{p}_0 \,, \, \mathbf{p}_1 - \mathbf{p}_0 \rangle = \langle \gamma(\varphi_*) \,, \, \gamma(\varphi_*) \rangle.$$

Replacing $\gamma(\varphi_*)$ by its expression (A.20), we write

$$||\mathbf{p}_1 - \mathbf{p}_0||^2 = \frac{1}{\omega^2} \left[2(1 - t_0) + (\bar{\tau}\varphi_*)^2 \right]$$

and since ω is greater than 0,

$$\omega = \frac{\sqrt{2(1 - t_0) + (\bar{\tau}\varphi_*)^2}}{||\mathbf{p}_1 - \mathbf{p}_0||}.$$

    In order to characterize φ_*, we consider the first two equations of (A.16). In the first equation, we have two cases. We start with

$$\langle \mathbf{p}_1 - \mathbf{p}_0 \,, \, \mathbf{t}_1 \times \mathbf{t}_0 \rangle = 0 \tag{A.40}$$

as the first case. It means that $D(\varphi_*)$ is equal to 0. In Section Appendix A.2.3, we will prove that the only two roots of D are the bounds of I_0,

$$D(\arccos t_0) = 0 \quad \text{or} \quad D(2\pi - \arccos t_0) = 0.$$

44

Thus, φ_* is either $\arccos t_0$ or $2\pi - \arccos t_0$. The value of N is then

$$N(\arccos t_0) = (1 - t_0)\sqrt{1 - t_0^2}$$

$$N(2\pi - \arccos t_0) = -(1 - t_0)\sqrt{1 - t_0^2},$$

from which we deduce with (A.16) that the value of φ_* is given by the sign of

$$\langle \mathbf{p}_1 - \mathbf{p}_0 \,,\, \mathbf{t}_1 + \mathbf{t}_0 \rangle.$$

As a conclusion, we write that if

$$\langle \mathbf{p}_1 - \mathbf{p}_0 \,,\, \mathbf{t}_1 \times \mathbf{t}_0 \rangle = 0,$$

then

$$\varphi_* = \begin{cases} \arccos t_0 & \text{if } \langle \mathbf{p}_1 - \mathbf{p}_0 \,,\, \mathbf{t}_1 + \mathbf{t}_0 \rangle > 0 \\ 2\pi - \arccos t_0 & \text{if } \langle \mathbf{p}_1 - \mathbf{p}_0 \,,\, \mathbf{t}_1 + \mathbf{t}_0 \rangle < 0. \end{cases}$$

Remark 1. *This case is actually a 2d case. Indeed, if the inner product (A.40) is equal to 0, then $\boldsymbol{p}_1$ and $\boldsymbol{p}_0$ are in the plane defined by the tangents. Furthermore, in this case, we can calculate the value of $\bar{\tau}$ which is equal to 0.*

Remark 2. *The case where the two inner products are equal to 0 can only happen when $\boldsymbol{p}_0 = \boldsymbol{p}_1$. We made the assumption that the two points were distinct.*

The second case is

$$\langle \mathbf{p}_1 - \mathbf{p}_0 \,,\, \mathbf{t}_1 \times \mathbf{t}_0 \rangle \neq 0.$$

Calculating the quotient of the first two lines of (A.16), we have

$$\frac{N(\varphi_*)}{D(\varphi_*)} = -\frac{(1 - t_0)\langle \mathbf{p}_1 - \mathbf{p}_0 \,,\, \mathbf{t}_1 + \mathbf{t}_0 \rangle}{\sqrt{2}|\langle \mathbf{p}_1 - \mathbf{p}_0 \,,\, \mathbf{t}_1 \times \mathbf{t}_0 \rangle|}. \tag{A.41}$$

In the following, we will write

$$H(\varphi_*) = \frac{N(\varphi_*)}{D(\varphi_*)} = -\chi$$

with

$$\chi = \frac{(1 - t_0)\langle \mathbf{p}_1 - \mathbf{p}_0 \,,\, \mathbf{t}_1 + \mathbf{t}_0 \rangle}{\sqrt{2}|\langle \mathbf{p}_1 - \mathbf{p}_0 \,,\, \mathbf{t}_1 \times \mathbf{t}_0 \rangle|}$$

45

which is a constant well-defined that only depends on $\mathbf{p}_0$, $\mathbf{p}_1$, $\mathbf{t}_0$ and $\mathbf{t}_1$.

We will see in Section Appendix A.2.3, that the equation

$$H(\varphi_*) = -\chi$$

has a unique solution. Ghosh restricted the domain of solutions to the interval

$$I_G = [\arccos t_0, \pi] \subsetneq I_0.$$

We will complete the study of H to the interval I_0.

To conclude this analysis, we have proven the unicity of the parameters φ_*, $\bar{\tau}$, ω and $\bar{\mathbf{\Omega}}$. Therefore, we have proven the unicity of the helix interpolating $\mathbf{p}_0$ and $\mathbf{p}_1$ with $\mathbf{t}_0$ and $\mathbf{t}_1$ as respective tangents, assuming that such a helix exists.

Synthesis. In this section, we prove that the helix interpolating the two points and the two tangents exists. To achieve this goal, we consider the parameters characterized in the analysis.

Consider the helix starting at $\mathbf{p}_0$ with the tangent $\mathbf{t}_0$ and with the parameters φ_*, $\bar{\tau}$, ω and $\bar{\mathbf{\Omega}}$ such that

$$\begin{cases} \bar{\tau} = \mathrm{sign}\langle \mathbf{p}_1 - \mathbf{p}_0 \,,\, \mathbf{t}_1 \times \mathbf{t}_0 \rangle \sqrt{\frac{t_0 - \cos \varphi_*}{1 - \cos \varphi_*}} \\ \omega = \frac{\sqrt{2(1-t_0) + (\bar{\tau}\varphi_*)^2}}{\|\mathbf{p}_1 - \mathbf{p}_0\|} \\ \bar{\mathbf{\Omega}} = \frac{1}{1+t_0} \left(\bar{\tau}(\mathbf{t}_1 + \mathbf{t}_0) + \left(\cot \frac{\varphi_*}{2} \right) (\mathbf{t}_1 \times \mathbf{t}_0) \right) \end{cases} \tag{A.42}$$

and

$$\begin{cases} H(\varphi_*) = -\chi & \text{if } \langle \mathbf{p}_1 - \mathbf{p}_0 \,,\, \mathbf{t}_1 \times \mathbf{t}_0 \rangle \neq 0, \\ \varphi_* = \arccos t_0 & \text{if } \langle \mathbf{p}_1 - \mathbf{p}_0 \,,\, \mathbf{t}_1 + \mathbf{t}_0 \rangle < 0, \\ \varphi_* = 2\pi - \arccos t_0 & \text{if } \langle \mathbf{p}_1 - \mathbf{p}_0 \,,\, \mathbf{t}_1 + \mathbf{t}_0 \rangle > 0. \end{cases}$$

Let us start with the case

$$\langle \mathbf{p}_1 - \mathbf{p}_0 \,,\, \mathbf{t}_1 \times \mathbf{t}_0 \rangle = 0.$$

In this case, we have

$$\varphi_* = \begin{cases} \arccos t_0 & \text{if } \langle \mathbf{p}_1 - \mathbf{p}_0 \,,\, \mathbf{t}_1 + \mathbf{t}_0 \rangle < 0 \\ 2\pi - \arccos t_0 & \text{if } \langle \mathbf{p}_1 - \mathbf{p}_0 \,,\, \mathbf{t}_1 + \mathbf{t}_0 \rangle > 0. \end{cases}$$

It is then very easy to check that we have

$$
\begin{cases}
\omega|\langle \mathbf{p}_1 - \mathbf{p}_0\,,\, \mathbf{t}_1 \times \mathbf{t}_0\rangle| = -\frac{\sqrt{2}(1-t_0)}{1-\cos\varphi_*}D(\varphi_*) \\
\omega\langle \mathbf{p}_1 - \mathbf{p}_0\,,\, \mathbf{t}_1 + \mathbf{t}_0\rangle = \frac{2}{1-\cos\varphi_*}N(\varphi_*)
\end{cases}
$$

and then that the helix satisfies the condition (A.16) of Lemma 5.2 and so interpolates the points $\mathbf{p}_0$ and $\mathbf{p}_1$ with respective tangents $\mathbf{t}_0$ and $\mathbf{t}_1$.

In the second case, we have

$$
\langle \mathbf{p}_1 - \mathbf{p}_0\,,\, \mathbf{t}_1 \times \mathbf{t}_0\rangle \neq 0.
$$

From the equality $H(\varphi_*) = -\chi$, we deduce

$$
\frac{N(\varphi_*)}{D(\varphi_*)} = -\frac{(1-t_0)\langle \mathbf{p}_1 - \mathbf{p}_0\,,\, \mathbf{t}_1 + \mathbf{t}_0\rangle}{\sqrt{2}|\langle \mathbf{p}_1 - \mathbf{p}_0\,,\, \mathbf{t}_1 \times \mathbf{t}_0\rangle|}
$$

that we can rewrite as

$$
\frac{\frac{2}{1-\cos\varphi_*}N(\varphi_*)}{\frac{\sqrt{2}(1-t_0)}{1-\cos\varphi_*}D(\varphi_*)} = -\frac{\langle \mathbf{p}_1 - \mathbf{p}_0\,,\, \mathbf{t}_1 + \mathbf{t}_0\rangle}{|\langle \mathbf{p}_1 - \mathbf{p}_0\,,\, \mathbf{t}_1 \times \mathbf{t}_0\rangle|}.
$$

It follows that there exists a strictly positive real μ such that

$$
\langle \mathbf{p}_1 - \mathbf{p}_0\,,\, \mathbf{t}_1 + \mathbf{t}_0\rangle = \frac{2\mu}{1 - \cos\varphi_*}N(\varphi_*)
$$

and

$$
|\langle \mathbf{p}_1 - \mathbf{p}_0\,,\, \mathbf{t}_1 \times \mathbf{t}_0\rangle| = -\mu\frac{\sqrt{2}(1 - t_0)}{1 - \cos\varphi_*}D(\varphi_*).
$$

Expressing $\mathbf{p}_1 - \mathbf{p}_0$ in the basis $\{\mathbf{e}_1, \mathbf{e}_2, \mathbf{e}_3\}$, we have

$$
\begin{aligned}
||\mathbf{p}_1 - \mathbf{p}_0||^2 \\
&= \langle \mathbf{p}_1 - \mathbf{p}_0\,,\, \mathbf{e}_1\rangle^2 + \langle \mathbf{p}_1 - \mathbf{p}_0\,,\, \mathbf{e}_2\rangle^2 \\
&= \frac{\langle \mathbf{p}_1 - \mathbf{p}_0\,,\, \mathbf{t}_1 \times \mathbf{t}_0\rangle^2}{1 - t_0^2} + \frac{\langle \mathbf{p}_1 - \mathbf{p}_0\,,\, \mathbf{t}_1 + \mathbf{t}_0\rangle^2}{2(1 + t_0)}.
\end{aligned} \tag{A.43}
$$

Developing (A.43) and replacing $\bar{\tau}^2$ by (A.42), we have

$$
||\mathbf{p}_1 - \mathbf{p}_0||^2 = \mu^2(2(1 - t_0) + \varphi_*^2\bar{\tau}^2),
$$

47

and then, since μ is positive

$$\mu = \frac{1}{\omega}.$$

Thus, the helix satisfies the conditions (A.13) of Lemma 5.2 and so interpolates $\mathbf{p}_0$ and $\mathbf{p}_1$ with respective tangents $\mathbf{t}_0$ and $\mathbf{t}_1$.

As a conclusion of the synthesis, we have proven that given two points and two tangents satisfying (A.1), there exists a unique short helix that interpolates the points and the tangents.

Appendix A.2.3. Studies of D and H
Study of D. We defined the function D on

$$I_0 = [\arccos t_0, 2\pi - \arccos t_0]$$

with

$$D(\varphi) = (\varphi \cos \frac{\varphi}{2} - 2 \sin \frac{\varphi}{2})\sqrt{t_0 - \cos \varphi}.$$

Since $\sqrt{t_0 - \cos \varphi}$ is strictly positive on the interior of I_0 and equal to 0 on the boundary, we consider the function

$$f(\varphi) = \frac{\varphi \cos \frac{\varphi}{2} - 2 \sin \frac{\varphi}{2}}{\sin \frac{\varphi}{2}} = (\varphi \cot \frac{\varphi}{2} - 2).$$

We have

$$f'(\varphi) = \frac{\varphi - \sin \varphi}{-1 + \cos \varphi}$$

which is strictly negative on $]0, 2\pi[$. So, the function f is strictly decreasing on $]0, 2\pi[$. And we have

$$\lim_{\varphi \to 0^+} f(\varphi) = 0$$

which implies that f is strictly negative on $]0, 2\pi[$ and thus on I_0. Since on the interior of I_0 we have

$$\sin \frac{\varphi}{2} > 0$$

it follows that D is strictly negative on the interior of I_0 and equal to 0 on the boundary.

Study of H. The study of H is a little bit more difficult because H depends on the parameter t_0 which is in the interval $]-1, 1[$. We are going to show

48

that for all values of t_0, H is strictly increasing on the interior of I_0, and that we have

$$\lim_{\varphi \to \arccos t_0^+} H(\varphi) = -\infty$$

$$\lim_{\varphi \to 2\pi - \arccos t_0^-} H(\varphi) = +\infty.$$

Thus, we will show that for any value of t_0, and any value of ψ, the equation

$$H(\varphi) = \psi$$

has a unique solution on the interior of I_0.

Let $t_0 \in]-1, 1[$. We have

$$N(\arccos t_0) = (1 - t_0)\sqrt{1 - t_0^2} > 0$$

$$N(2\pi - \arccos t_0) = -(1 - t_0)\sqrt{1 - t_0^2} < 0,$$

and

$$D(\arccos t_0) = 0$$
$$D(2\pi - \arccos t_0) = 0$$
$$D(\varphi) < 0 \qquad\qquad \forall \varphi \in]\arccos t_0, 2\pi - \arccos t_0[$$

so we deduce

$$\lim_{\varphi \to \arccos t_0^+} H(\varphi) = \lim_{\varphi \to \arccos t_0^+} \frac{N(\varphi)}{D(\varphi)} = -\infty$$

$$\lim_{\varphi \to 2\pi - \arccos t_0^-} H(\varphi) = \lim_{\varphi \to 2\pi - \arccos t_0^-} \frac{N(\varphi)}{D(\varphi)} = +\infty.$$

In order to prove that H is strictly increasing, we study the sign of its derivative on $\overset{\circ}{I_0}$, the interior of I_0. We have

$$H'(\varphi) = -\frac{(1 + t_0)\sin\frac{\varphi}{2}}{2D^2(\varphi)\sqrt{t_0 - \cos\varphi}}(h_0(\varphi)t_0 + h_1(\varphi)) \qquad\qquad (A.44)$$

49

with

$$h_0(\varphi) = 4 - \varphi^2 - 4\cos\varphi - \varphi\sin\varphi$$
$$h_1(\varphi) = -1 + \cos 2\varphi + \varphi\sin\varphi + \varphi^2\cos\varphi.$$

Since we have

$$-\frac{(1+t_0)\sin\frac{\varphi}{2}}{2D^2(\varphi)\sqrt{t_0 - \cos\varphi}} < 0$$

we study the sign of the two variable function

$$F(t, \varphi) = h_0(\varphi)t + h_1(\varphi)$$

on the domain

$$\mathcal{E} = \left\{ (t, \varphi), \begin{array}{l} t \in [-1, 1] \\ \varphi \in [\arccos t, 2\pi - \arccos t] \end{array} \right\}.$$

The space $\mathcal{E}$ is closed and bounded because we have

$$\mathcal{E} = f^{-1}(]-\infty, 0]) \cap ([-1, 1] \times [0, 2\pi])$$

where f, such that

$$f(t, \varphi) = \cos\varphi - t,$$

is a continuous function on $\mathbb{R}^2$.

Since F is also a continuous function on the compact space $\mathcal{E}$, $F(\mathcal{E})$ is a compact. Particularly, F attains its maximum. Therefore, if F attains its maximum on the interior of $\mathcal{E}$, it will be at a critical point, since this global maximum will also be local. Let us calculate the gradient of F:

$$\frac{\partial F}{\partial t} = h_0(\varphi)$$
$$\frac{\partial F}{\partial \varphi} = h_0'(\varphi)t + h_1'(\varphi).$$

We have

$$h_0(\varphi) = 4 - \varphi^2 - 4\cos\varphi - \varphi\sin\varphi$$
$$h_0'(\varphi) = -2\varphi - \varphi\cos\varphi - 3\sin\varphi$$
$$h_0''(\varphi) = -2 + 2\cos\varphi + \varphi\sin\varphi$$
$$h_0'''(\varphi) = \varphi\cos\varphi - \sin\varphi$$
$$h_0''''(\varphi) = -\varphi\sin\varphi.$$

and we can sum up the variations of h_0 in this table

x	0	π	$\varphi_\#$	2π
$h_0''''(x)$	$-$	$+$	$+$	

where $\varphi_\#$ is such that $h_0'''(\varphi_\#) = 0$. Thus h_0 is strictly decreasing on $[0, 2\pi]$ equal to 0 at 0 so h_0 strictly negative on $]0, 2\pi[$. We conclude that the gradient of F cannot be equal to 0 on the interior of $\mathcal{E}$.

Therefore, F attains its maximum on the boundary of $\mathcal{E}$ that we write as

$$\partial\mathcal{E} = \mathcal{F}_1 \cup \mathcal{F}_2 \cup \mathcal{F}_3 \cup \mathcal{F}_4$$

where

$$\mathcal{F}_1 = \left\{ (t, \varphi), \begin{array}{l} t \in [-1, 1] \\ \varphi = \arccos t \end{array} \right\}$$

$$\mathcal{F}_2 = \left\{ (t, \varphi), \begin{array}{l} t \in [-1, 1] \\ \varphi = 2\pi - \arccos t \end{array} \right\}$$

$$\mathcal{F}_3 = \left\{ (t, \varphi), \begin{array}{l} t = -1 \\ \varphi \in [\pi, \pi] \end{array} \right\}$$

$$\mathcal{F}_4 = \left\{ (t, \varphi), \begin{array}{l} t = 1 \\ \varphi \in [0, 2\pi] \end{array} \right\}$$

Let us study F on $\mathcal{F}_1$. Replacing φ by $\arccos t$ in F, we have

$$F_1(t) = (1 - t)(-2 + 2t + \sqrt{1 - t^2} \arccos t).$$

Let

$$f_1(t) = -2 + 2t + \sqrt{1 - t^2} \arccos t$$
$$g_1(x) = -2 + 2 \cos x + x \sin x.$$

We have

$$f_1(t) = g_1(\arccos t)$$

and we identify

$$g_1(x) = h_0''(x).$$

Since h_0'' is strictly negative on $]0, \pi]$ and reaches 0 at 0. So, we can write that f_1 is strictly negative on $[-1, 1[$ and is equal to 0 at 1 and so is F_1.

Now, let us study F on $\mathcal{F}_2$. Replacing φ by $2\pi - \arccos t$ in F, we obtain

$$F_2(t) = (1 - t)(-2 + 2t - \sqrt{1 - t^2}(2\pi - \arccos t)).$$

Let us write

$$f_2(t) = -2 + 2t - \sqrt{1 - t^2}(2\pi - \arccos t)$$
$$g_2(x) = -2 + 2 \cos x + x \sin x.$$

We have
$$f_2(t) = g_2(2\pi - \arccos t)$$
and we conclude as previous that F_2 is strictly negative on $[-1, 1[$ and equal to 0 at 1.

Now, we study F on $\mathcal{F}_3$ which is a singleton.

$$\begin{aligned} F(-1, \pi) = &- 4 + \pi^2 + 4\cos\pi + \pi\sin\pi \\ &- 1 + \cos 2\pi + \pi\sin\pi + \pi^2\cos\pi \\ = &- 8 \end{aligned}$$

Now, there is only one case remaining, we study F on $\mathcal{F}_4$. Replacing t by 1 in F, we have

$$\begin{aligned} F_4(\varphi) &= 3 - \varphi^2 - 4\cos\varphi + \cos 2\varphi + \varphi^2\cos\varphi \\ &= (\cos 2\varphi - 1) + (4 - \varphi^2)(1 - \cos\varphi). \end{aligned}$$

Since we have

$$\begin{aligned} \cos 2\varphi - 1 = -2\sin^2\varphi &= -4\sin^2\frac{\varphi}{2}\cos^2\frac{\varphi}{2} \\ &= -8\sin^2\frac{\varphi}{2}(\frac{\cos\varphi + 1}{2}) \end{aligned}$$

and

$$1 - \cos\varphi = 2\sin^2\frac{\varphi}{2}$$

we write

$$F_4(\varphi) = 2\sin^2\frac{\varphi}{2}(2 - \varphi^2 - 2\cos\varphi).$$

Let

$$g_4(\varphi) = 2 - \varphi^2 - 2\cos\varphi,$$

we have

$$\begin{aligned} g_4'(\varphi) &= -2\varphi + 2\sin(\varphi) = 0 \text{ at } 0 \\ g_4''(\varphi) &= -2 + 2\cos\varphi \; < 0 \quad \text{on }]0, 2\pi[. \end{aligned}$$

So g_4' is strictly decreasing on $[0, 2\pi]$ and so is negative on $]0, 2\pi]$. Since we have $g_4(0) = 0$, g_4 is strictly negative on $]0, 2\pi]$ and equal to 0 at 0 and so is F_4.

To conclude, we have shown that F is negative on $\partial\mathcal{E}$ and strictly negative on the interior of $\mathcal{E}$, and so we have

$$\forall t \in]-1,1[, \ \forall\varphi \in \overset{\circ}{I_0}, \ h_0(\varphi)t_0 + h_1(\varphi) < 0.$$

It follows, with (A.44) that

$$\forall t \in]-1,1[, \ \forall\varphi \in \overset{\circ}{I_0}, \ H'(\varphi) > 0.$$

Finally, for any value of t_0, H strictly is increasing on $\overset{\circ}{I_0}$. It implies that H is a bijection from $\overset{\circ}{I_0}$ to $\mathbb{R}$ which means that for any value of t_0, and any value of ψ,

$$H(\varphi) = \psi$$

has a unique solution on $\overset{\circ}{I_0}$.